sustainability

MDPI

Article

Systemic Spatial Inequalities in China's Elderly Care: Multi-Scale Diagnostic Evidence for Sustainable Healthy Landscapes in a Monocentric Metropolitan Region

Jiajun Xu [1,2], Wanying Liao [3,4], Hongbin Zhang [5], Noor Hashimah Hashim Lim [6,*] and Chng Saun Fong [1,7,*]

1 Institute for Advanced Studies, Universiti Malaya, Kuala Lumpur 50603, Malaysia; jiajunxu2000@gmail.com
2 United College, The Chinese University of Hong Kong, Hong Kong 999077, China
3 Guangdong Institute of Arts and Sciences, Lianjiang 524400, China; wanyingliao1998@gmail.com
4 Faculty of Arts and Social Sciences, Universiti Malaya, Kuala Lumpur 50603, Malaysia
5 School of Management, Zhejiang University, Hangzhou 310058, China; hongbin_zhang323@163.com
6 International Institute of Public Policy and Management, Universiti Malaya, Kuala Lumpur 50603, Malaysia
7 China-Malaysia International Institute for Advanced Studies, Universiti Malaya, Kuala Lumpur 50603, Malaysia
* Correspondence: shimalim@um.edu.my (N.H.H.L.); fongcs92@um.edu.my (C.S.F.)

Abstract

Population aging is reshaping regional health systems, but the decisive variable is not only aggregate capacity—it is where care is placed. Optimization studies often reduce spatial imbalance to technical inefficiency, leaving the structural and institutional production of inequality unexamined, with less-developed regions remaining largely marginalized in spatial scholarship. Applying a structural–locational nexus to China's Wuhan "1+8" City Circle—a monocentric metropolitan region with a steep urban–rural gradient—this study integrates multi-scale exploratory spatial analysis to diagnose system-wide and subunit-level structures and identify typology-specific density hotspots, thereby quantifying variation across service, organizational, and functional classifications. The multi-scale diagnosis reveals a "monocentric collapse" (system-wide CV = 102.67%), where extreme internal fragmentation in core urban districts (CV = 223.66%) coexists with structural marginality in sparsely covered rural counties (CV = 95.33%). Crucially, this spatial polarization is likely structured by institutional divergence: social organizations exhibit extreme core concentration driven by market-oriented spatial selectivity (CV = 238.03%) despite nonprofit mandates, whereas facilities operated by government organizations approximate a random-like, geographically dispersed administrative scaffolding (CV = 57.95%), serving as the only reliable spatial anchor for peripheral regions. Functional differentiation further demonstrates that high-intensity facilities remain heavily clustered in the primary center, whereas elderly apartments selectively anchor across sub-centers. These findings reframe spatial inequality not as an incidental planning failure, but as a systemic structural outcome of territorial governance that constrains sustainable eldercare development. Achieving sustainable healthy landscapes under rapid population aging requires spatially targeted interventions—steering market forces toward underserved peripheries; implementing functionally differentiated planning standards; reinforcing a three-tier public network to remedy rural structural deficits; and establishing cross-jurisdictional coordination.

Keywords: spatial inequality; elderly care facilities; exploratory spatial data analysis; institutional divergence; sustainable healthy landscapes

Check for updates

Academic Editors: Raymond A. Tutu, Jones Kwaku Adjei and Henry N. N. Bulley

Received: 15 October 2026
Revised: 3 November 2026
Accepted: 5 November 2026
Published: 9 November 2026

Copyright: © 2026 by the authors. Licensee MDPI, Basel, Switzerland. This article is an open access article distributed under the terms and conditions of the Creative Commons Attribution (CC BY) license.

1. Introduction

Place fundamentally conditions health, and urban environments mediate population health outcomes; persistent intra- and inter-urban health disparities therefore link equitable access to urban services and coherent urban planning with observed inequalities in population health, making equitable design central to population well-being [1]. Population aging is an irreversible global trend that pressures welfare systems and forces spatial (re)organization of elderly care provision [2]. As older populations' basic and latent needs intensify and diversify [3], equitable and sustainable public eldercare depends not only on aggregate service capacity [4] but on the spatial allocation of elderly care facilities (ECFs) across heterogeneous territories [5–9]. Aging is spatially differentiated, yet policy and planning continue to prioritize aggregate supply targets [10,11]. A lack of attention to spatial differentiation is associated with uneven service provision and may constrain access to care; it has also been linked to broader social disparities and may pose challenges to system-wide sustainability [12].

Studies document availability and accessibility inequities within cities [13–18] and between urban and rural areas [19], consistently showing uneven facility distribution, regional inequalities in spatial availability [14,20–24], and demand–supply misalignment [25–30]. However, most studies frame spatial imbalance as a modeling problem [31]—a technical inefficiency correctable through optimization, capacity expansion, or generic policy adjustment—thereby confining inquiry to empirical modeling and obscuring structural, normative, and institutional dimensions [32,33]. In welfare-oriented systems, public provision is not merely a technical matter; it is also discussed in relation to (re)distributive justice and equitable access to care [33,34]. Despite increasingly sophisticated measurement of locational gaps and allocation patterns [35–38], research remains largely technocratic and data-driven, with comparatively limited attention to governance systems and socioeconomic logics.

China, with the world's largest older population and one of the fastest aging trajectories, is projected by UN *World Population Prospects 2022* to account for nearly one-quarter of the global older population by 2050 [39]. Rapid, multidimensional aging already challenges public resource allocation and social security [40]. China has not yet reached peak aging; projections place the steepest increase around the 2030s–2040s [41], making the coming decade a critical window for policy response. Despite growing policy attention, substantial regional and urban–rural inequalities in eldercare resources persist, including stark disparities in institutional provision [40]. China's vast territory, large older population, and rapid aging help explain why Chinese scholarship has come to dominate global spatial-perspective research on ECFs.

Rooted in a socialist governance framework that normatively emphasizes reducing spatial inequality, people-centered development, and common prosperity, China treats eldercare as a justice issue as well as a demographic challenge; national strategies [42–44]—"Equalization of Basic Public Services" and "Actively Responding to Population Aging (Proactively Addressing Population Aging)"—reflect this orientation [45,46]. Despite this normative commitment, empirical research remains concentrated on national scales, economically advanced regions, and intra-urban contexts characterized by dense academic institutions, concentrated funding, and higher socioeconomic development [47]. This geographical and institutional bias limits generalizability by marginalizing the "places that don't matter" [47,48] and leaves an understanding void regarding less-developed or peripheral settings.

Specifically, urban agglomerations remain rare analytical units, and the spatial and systemic logic of eldercare welfare landscapes in monocentric metropolitan contexts remains rarely interrogated. To address these gaps, this study focuses on the Wuhan City Circle (WCC), an urban agglomeration spanning a wide urban-to-rural development gradient.

Within this monocentric metropolitan context, what welfare geography of eldercare services in central China is revealed? To answer this question, the study advances exploratory spatial data analysis (ESDA) as a diagnostic framework, integrating multi-scale spatial analysis with hierarchical facility classification. The study adopts a structural diagnostic perspective, moving beyond descriptive mapping to examine not only where deficiencies exist but how spatial imbalances are (re)produced and translated into welfare outcomes. This overarching question is operationalized through three questions:

i. What is the system-wide macro-scale and hierarchical subunit-level spatial structure of welfare ECFs in the WCC? At the metropolitan scale, does area variability of global Voronoi cells indicate a clustered, random, or regular pattern? Within the urban–rural administrative hierarchy, how does variability of administratively clipped Voronoi areas differ across tiers?
ii. Beyond system-wide and tier-level structure, do ECF types exhibit distinct density geographies across analytically specified scales? Under bandwidth-based multi-scale parameterization, where are high-density clusters (hotspots) of different ECF types across the metropolitan area?
iii. Synthesizing system-wide, tier-level, and type-specific exploratory results, how does spatial characterization vary by service mode, organizational mode, and functional type, and what policy implications do these variations have for hierarchical differentiation, distributional balance, and sustainable development of welfare eldercare systems?

Together, these questions use spatial differentiation and provision imbalances as a diagnostic entry point for examining spatial patterns relevant to sustainability in welfare eldercare provision. By interpreting spatial inequalities in service provision as potentially structured by hierarchical service systems, the study contributes to debates on welfare governance under rapid population aging. Rather than treating uneven spatial patterns as incidental planning outcomes, it examines whether such patterns are associated with systemic features of territorial governance structures. Its contribution lies in moving spatial assessment beyond conventional metrics and uniform supply targets through a structural–locational diagnosis of hierarchical service systems.

2. Materials and Methods

2.1. Description of the Study Area

This study examines the WCC, also known as the Wuhan "1+8" City Circle (Wuhan Metropolitan Area), a rapidly urbanizing mega-region in central China (Figure 1). Characterized by a pronounced core–periphery socioeconomic gradient—from the metropolitan core of Wuhan to its eight surrounding, less-developed prefecture-level cities—the WCC, a monocentric metropolitan context, encapsulates the intricate urban–rural continuum and administrative complexity typical of contemporary Chinese city-regions [47,49,50].

Administratively, the WCC comprises nine cities directly governed by Hubei Province: the prefecture-level cities of Wuhan, Huangshi, Ezhou, Xianning, Xiaogan, and Huanggang, and the county-level cities of Tianmen, Qianjiang, and Xiantao [49–52]. To analyze welfare ECF distribution at a fine scale, the study uses the region's 48 county-level units. This administrative heterogeneity—urban districts (core and peripheral), county-level cities (directly governed and general), and rural counties (Figure 2)—establishes the WCC as an ideal case for interrogating the equality dimensions of ECF distribution. Moving beyond a conventional three-tier classification, the study employs a refined five-level urban–rural hierarchy to capture the intra-regional spatial structure shaping eldercare provision. This hierarchy integrates administrative rank with functional centrality to examine intra-regional disparities in public service distribution. The five tiers are:

(I) **Core Urban Districts**: The metropolitan nucleus, with the highest administrative–economic concentration and mature urbanization;
(II) **Peripheral Urban Districts**: Transitional zones with mixed urban–suburban functions, often absorbing decentralized activities from the core;
(III) **Directly Governed County-Level Cities**: Special-status cities under provincial administration, with greater fiscal and planning autonomy;
(IV) **General County-Level Cities**: Semi-urban hubs under prefecture-level jurisdiction, serving as secondary growth poles;
(V) **Rural Counties**: Areas dominated by agricultural and ecological functions, with minimal urban infrastructure.

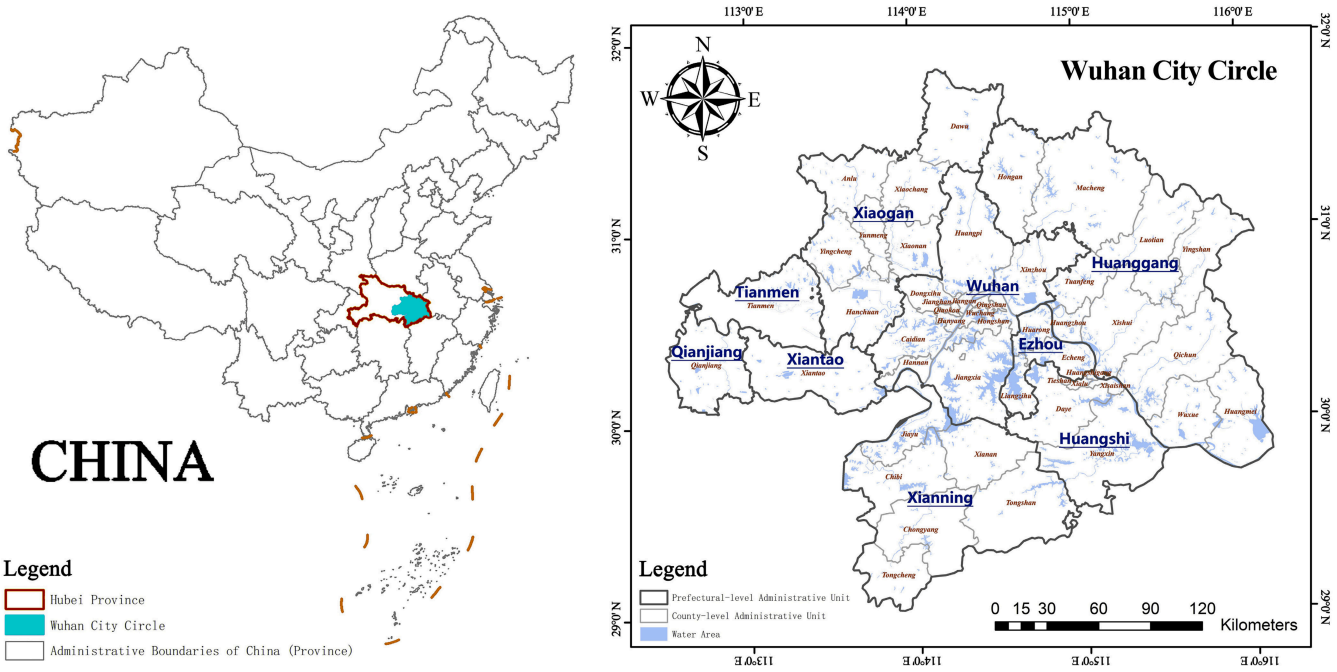


Figure 1. Location and administrative extent of the WCC. [Note: Chinese Drawing Review No. GS (2024) 0650; projection: WGS 1984 UTM Zone 49N].

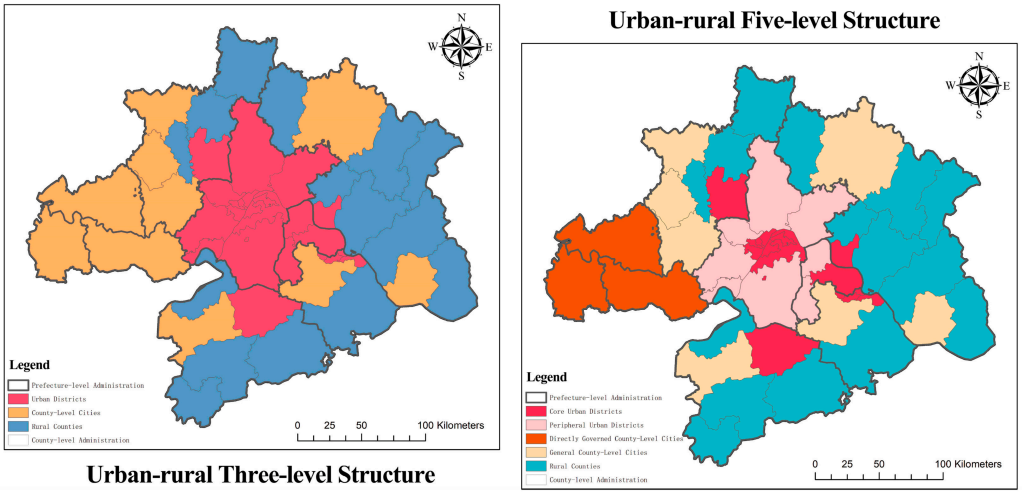


Figure 2. Multi-tier urban–rural administrative hierarchy of the WCC, central China.

2.2. Data Sources and Preprocessing

Urbanization and rural development have expanded opportunity and improved welfare, but their acceleration has generated systemic challenges [53]; addressing entrenched

disadvantages in underserved areas increasingly depends on coordinating public, nonprofit, and commercial actors within urban development initiatives [47,54]. Accordingly, the analysis focuses on welfare-oriented ECFs in the WCC, drawing on geocoded locations and attribute data integrated with administrative boundary datasets.

Facility data, as of 10 June 2024, comprise entities registered under two institutional frameworks in China: public institutions at various government levels and private non-enterprise units supervised by civil affairs departments at corresponding administrative levels. Welfare status is defined by a nonprofit mandate—profit not the primary purpose—across the full construction and operation cycle [47]. Official sources included the Hubei Provincial Department of Civil Affairs and the municipal civil affairs portals of Wuhan, Ezhou, Xiaogan, Huanggang, Xianning, Huangshi, Xiantao, Qianjiang, and Tianmen. Records were cross-checked against China's principal commercial registration and public-disclosure platforms—Aiqicha (https://aiqicha.baidu.com/) and Tianyancha (https://www.tianyancha.com/).

Attributes collected for each facility include name, geographic address, main function, type, unified social credit code, organizational head, establishment date (if applicable), and registered capital (if applicable). Facilities were classified by service mode, organizational mode, and functional type to capture internal differentiation within the welfare eldercare system. Registered addresses were geocoded using the Baidu Map Geocoding API and converted to WGS 1984. Registration attributes—unified social credit code, establishment date, registered capital, and organizational head—were cross-checked against the commercial platforms noted above.

All facility geo-data underwent systematic collection, screening, verification, and organization (Figure 3), with location verification as a critical step. Location verification preserved all 976 facility points at their original geocoded coordinates, including 58 instances of coordinate overlap representing distinct entities sharing a single physical address or building complex—a common scenario in multi-tenant or campus-style settings. Preserving these positional relationships over artificial dispersion ensures that the spatial analysis accurately reflects the consolidated nature of real-world eldercare resource distribution.

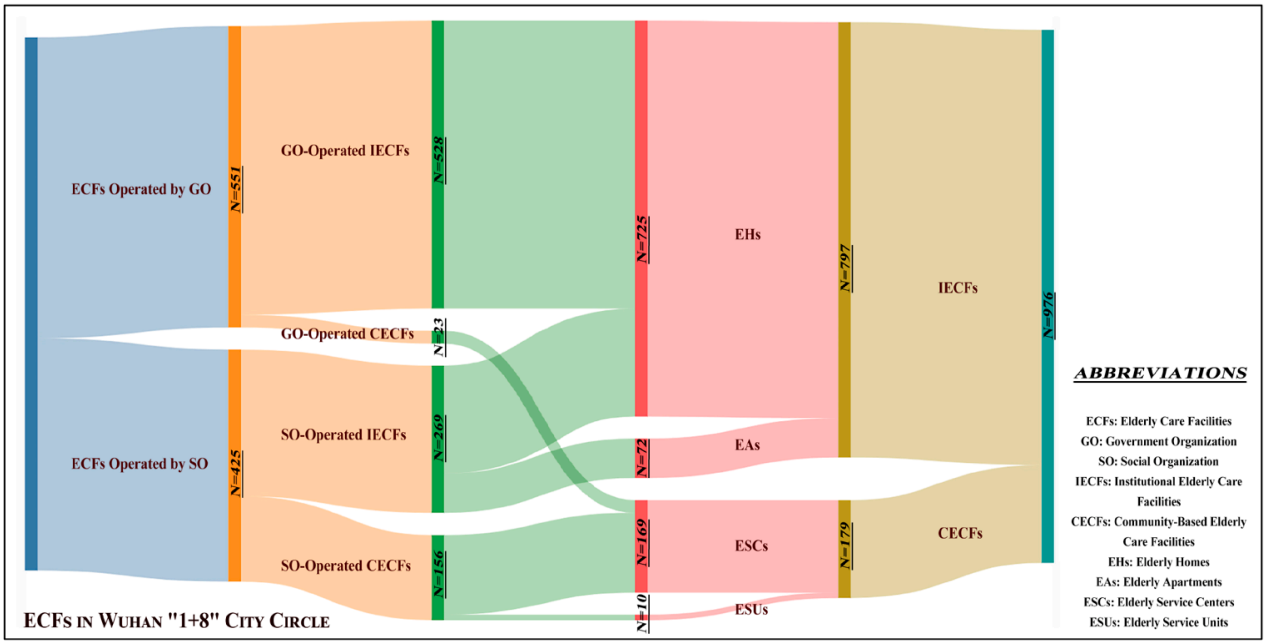


Figure 3. Sankey diagram of the processed dataset.

2.3. Study Design and Methods

2.3.1. System-Wide and Tier-Level Voronoi Structure

The Voronoi diagram (VD) provides a deterministic geometric representation of nearest-facility partitioning; the area variability of its Thiessen polygons serves as a proxy for spatial heterogeneity in potential service areas. Construction begins with Delaunay triangulation; perpendicular bisectors of each triangle edge form polygon edges, and their intersections define polygon vertices [55–57]. The coefficient of variation (CV) is used to classify the spatial structure of facility distribution: clustered if CV > 64%, random if 33% ≤ CV ≤ 64%, and regular if CV < 33% [56,57].

Let the study region be R, and let all target facilities within the region form a point set $P = \{p_1, p_2, \ldots, p_n\}$. For any spatial location $x \in R$, the Euclidean distance to facility p_i is $d(x, p_i)$. The global Voronoi cell $V(p_i)$ is defined as:

$$V(p_i) = \{x, \in R | d(x, p_i) \leq d(x, p_j)\ \forall j \neq i\} \tag{1}$$

Let $S_i^{\text{global}} = \text{Area}(V(p_i))$ denote the global Voronoi cell area of facility p_i without administrative boundary constraints; this area is interpreted as a geometric proxy for the facility's potential service area. The degree of variation in the global spatial distribution, termed the global CV, is defined as:

$$CV_{\text{global}} = \frac{\sqrt{\frac{1}{n}\sum_{i=1}^{n}\left(S_i^{\text{global}} - \overline{S}^{\text{global}}\right)^2}}{\overline{S}^{\text{global}}} \times 100\% \tag{2}$$

where $\overline{S}^{\text{global}}$ is the mean global Voronoi cell area. CV_{global} describes the macro-scale variability of nearest-facility partitioning across the region under a pure distance-competition assumption. It serves as a contextual benchmark for subsequent stratified analyses but is not compared directly with tier-specific CVs, because the latter are based on administratively clipped fragments with different spatial units and area definitions.

To move beyond a region-wide view and examine the spatial logic of eldercare provision, a stratified analytical framework is employed. Building on the conventional tripartite classification of county-level units (urban districts, county-level cities, rural counties), a refined five-tier urban–rural hierarchy tailored to the WCC's developmental gradient is introduced (Figure 2).

Notably, the VD tessellation—which partitions space by proximity to facilities—is spatially intersected with county-level administrative boundaries, creating hybrid analytical units that reflect both service proximity and formal jurisdiction. Let $A = \{A_1, A_2, \ldots, A_M\}$ denote the set of M administrative units. The global Voronoi cells are intersected with these boundaries to produce administratively clipped Voronoi polygons:

$$F_{i,k} = V(p_i) \cap A_k,\ \forall i \in \{1, \ldots, n\},\ \forall k \in \{1, \ldots, M\} \tag{3}$$

where $S_{i,k} = \text{Area}(F_{i,k})$ denotes the administratively clipped Voronoi area of facility p_i within administrative unit A_k, interpreted as a geometric proxy for potential service area within that unit. A polygon is retained as valid if $S_{i,k} > 0$. This operation preserves the geometric assignment of all cross-boundary facilities, thereby avoiding selection bias from discarding boundary facilities. A single facility's global Voronoi cell may intersect multiple administrative units, generating multiple polygons assigned to their respective units.

CV analysis is not applied uniformly but separately within each of the three or five hierarchical levels. For any level $l \in L$, the set of all valid polygon areas within that level is:

$$S_l = \{S_{i,k}, | A_k \in l\ S_{i,k} > 0\} \tag{4}$$

Each level-specific CV is then defined as:

$$CV_l = \frac{\sqrt{\frac{1}{N_l}\sum_{S \in S_l}(S - \overline{S}_l)^2}}{\overline{S}_l} \times 100\% \quad (5)$$

where $N_l = |S_l|$ is the total number of valid Thiessen polygons (after spatial intersection with administrative boundaries) assigned to level l, and $\overline{S}_l$ is the mean polygon area. CV_l measures the relative dispersion of administratively clipped Voronoi areas within a given urban–rural tier, i.e., the degree of spatial heterogeneity in geometric potential service areas. Because a single facility's Voronoi cell may intersect multiple administrative units, the sum of N_l across all levels exceeds the total number of facilities n.

Tier-level CVs are compared directly to assess the relative strength of geometric spatial heterogeneity across urban–rural tiers. A higher CV_l indicates greater relative dispersion of clipped Voronoi areas within that tier, and thus stronger geometric spatial heterogeneity; a lower CV_l indicates weaker heterogeneity. For example, CV = 250% in core urban districts versus 95% in rural counties indicates stronger fragmentation and heterogeneity of clipped Voronoi areas in urban districts.

Notably, the major urban–rural tiers contain sufficient valid clipped Thiessen polygons. Inter-tier CV comparison is therefore treated as a descriptive structural comparison with adequate polygon counts, not as a formal statistical test, and is used to reveal systematic differences in the geometric structure of potential service areas along the urban–rural gradient. Within the same tier, administrative units are relatively consistent in area and shape (e.g., core urban districts are generally small, rural counties generally large in China). Systematic geometric differences between tiers are insufficient to account for large inter-tier CV gaps, if any. Large inter-tier CV differences are therefore interpreted as structural differences in the geometric heterogeneity of potential service areas across the urban–rural gradient, not as artifacts of polygon counts alone. Residual geometric effects from administrative unit area and shape, however, warrant cautious interpretation.

2.3.2. Detecting Localized Spatial Density Concentrations

To complement the system-wide and tier-level structural characterization by revealing where concentrations occur, Kernel Density Estimation (KDE) is employed to delineate high-density clusters (hotspots) of different facility types. Among hotspot delineation methods for spatial point elements, density analysis—comprising point density and kernel density—is widely used [55]. Point density requires a user-specified neighborhood to calculate pixel-wise density, whereas kernel density spreads a known total number of points outward from each point location [55]. Unlike point density, kernel density produces continuous, smooth hotspot regions rather than dispersed individual density peaks [55]. Accordingly, KDE is adopted to identify spatial hotspots of ECFs, as it reduces interference from local fluctuations, captures overall hotspot trends, and remains sensitive to density gradients.

As a nonparametric method, KDE reflects the central agglomeration strength of hotspot areas [52,58–61]. The predicted density at location (x,y) is given by [62,63]:

$$K_{\text{Density}} = \frac{1}{(\text{radius})^2}\sum_{i=1}^{n}\left[\frac{3}{\pi}\cdot\left(1-\left(\frac{\text{dist}_i}{\text{radius}}\right)^2\right)^2\right], \text{dist}_i < \text{radius} \quad (6)$$

where n is the number of input points within the search radius of (x,y); dist_i is the distance between point i and (x,y); a quartic kernel was implemented [56,62–64]. All computations used planar distances in WGS 1984 UTM Zone 49N, and density is expressed as facilities per km^2.

Manual definition of bandwidth and cell size was employed to replace software defaults, ensuring cross-type comparability. Standard default cell sizes (algorithmically

derived from the overall spatial extent by ArcGIS Desktop 10) computed to approximately 1253 m for the WCC—too coarse for fine-grained spatial analysis, as it obscures local variations and masks secondary agglomeration centers. Furthermore, default bandwidths are computed separately for each facility type based on its own distribution; such type-specific defaults would confound cross-type comparisons with differences in smoothing scale. A common fixed bandwidth across types and tiers removes this source of confounding and ensures density surfaces are compared under the same smoothing regime [65,66]. While adaptive bandwidths vary smoothing with local density and are desirable for estimating a single surface, they are undesirable when the objective is cross-type comparability [67].

A scale-explicit parameterization was implemented with bandwidths of 10 km (micro), 20 km (meso), and 30 km (macro), and corresponding cell sizes of 250 m, 500 m, and 750 m. This 40:1 ratio maintains internal consistency and balances spatial detail against surface smoothness. Scale choices were empirically anchored in average nearest neighbor (ANN) results for the WCC (Euclidean distance). For n facility points $p_1,\ldots,p_n$, the observed mean nearest neighbor distance is:

$$\overline{d}_{\text{obs}} = \frac{1}{n}\sum_{i=1}^{n} \min_{j \neq i} \| p_i - p_j \| \quad (7)$$

where $\|p_i - p_j\|$ is the Euclidean distance between points i and j, and each point is matched to its single nearest neighbor. For the pooled ECF set, $\overline{d}_{\text{obs}} = 3383.8$ m; type-specific $\overline{d}_{\text{obs}}$ ranged from 1799.2 m to 8764.8 m (Table 1).

Table 1. ANN distances of ECFs by classification.

Tier Comparison	Classification of ECFs	*N*	Observed Mean Distance (m)
	All ECFs	976	3383.8054
Service Mode	IECFs	797	4138.7560
	CECFs	179	3402.9583
Organizational Mode	ECFs Operated by GO	551	5911.8544
	ECFs Operated by SO	425	2178.3871
Functional Type	EHs	725	4559.3820
	EAs	72	8764.7747
	ESCs	169	3604.3563
	ESUs	10	1799.1644

The 10-km bandwidth exceeds the upper bound of this type-specific range, ensuring that even the most dispersed functional category is represented as a continuous surface rather than point-level peaks; 20 km and 30 km resolve metropolitan subcenters and regional concentration corridors, respectively. This anchoring rests on the established link between nearest neighbor distances and density-estimation bandwidths: nearest neighbor distances reflect local point spacing, and their theoretical basis in bandwidth selection is well developed [68]. In applied point-pattern analysis, K-order mean nearest neighbor distances have been used directly as KDE bandwidths [69], and nearest-neighbor-based bandwidths are standard options in point-pattern software [65,66]. This anchoring provides a defensible lower bound for surface construction but does not imply a uniquely optimal bandwidth; KDE remains scale-dependent [65–69].

The three bandwidths were used to examine how the overall density pattern—rather than the precise location of individual hotspot patches—changes with scale. At 10 km, the surface resolves micro-level clustering and fine-grained local peaks; at 20 km, these peaks coalesce into city subcenters; at 30 km, the surface captures metropolitan concentration corridors or the broad monocentric structure. Because the dispersion of a kernel density surface

is controlled by its bandwidth, the three surfaces are interpreted as scale-dependent expressions of the same underlying point pattern rather than as competing estimates of a single true pattern [65–69]. Across the three scales, the spatial pattern remains identifiable, while local fragmentation decreases as bandwidth increases. This scale-explicit parameterization reveals how eldercare provision concentrations differ across metropolitan scales.

In summary, the analysis follows an ESDA framework that combines two diagnostics—Voronoi-based heterogeneity measures and multi-scale KDE—to characterize the spatial characteristics of ECFs across scales and hierarchical tiers (Figure 4). ANN (observed mean nearest neighbor distance) serves solely to anchor KDE bandwidth selection and is not reported as a separate test of the global point pattern. Synthesized across spatial scales and facility hierarchies, this integrative interpretation moves to understanding how spatial pattern is (re)produced through hierarchical misalignment and territorial governance.

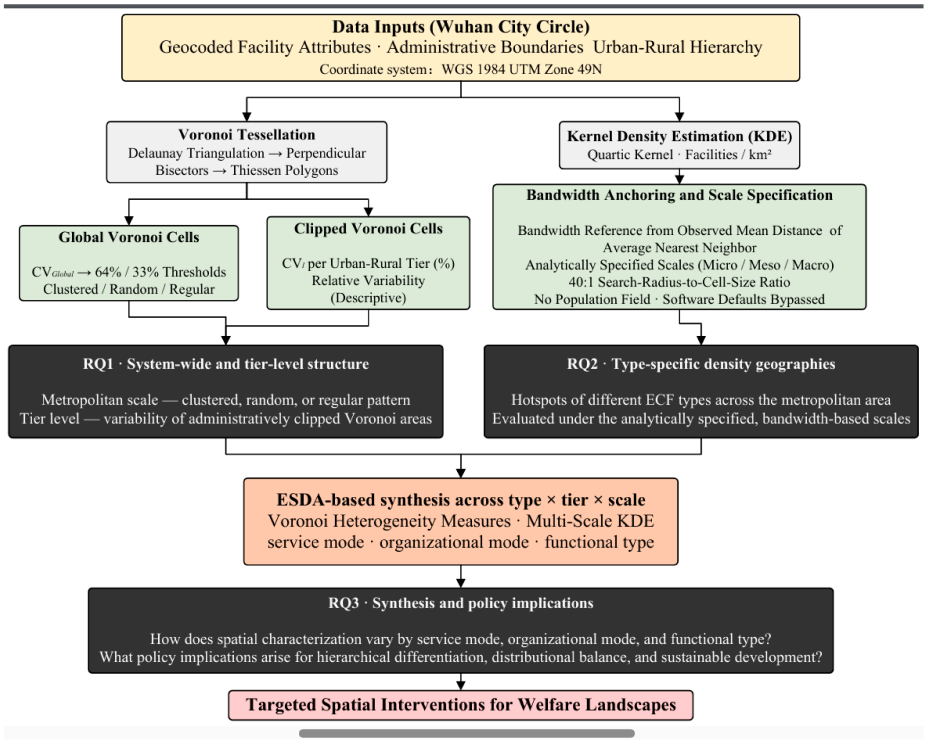


Figure 4. Analytical workflow of the ESDA-based spatial diagnostics.

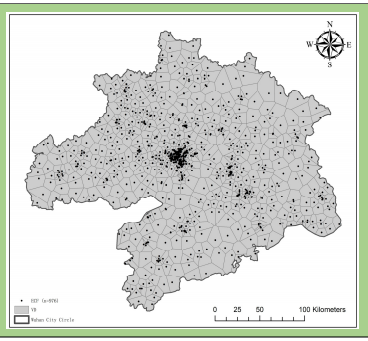
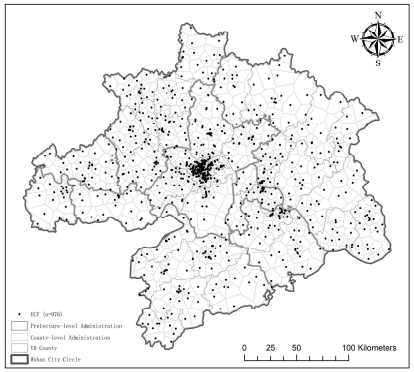
3. Results and Findings

3.1. Structural Patterns: System-Wide and Subunit-Level

3.1.1. All Welfare-Oriented ECFs

The CV of Thiessen polygon areas revealed pronounced spatial heterogeneity in welfare ECFs at both system-wide and subunit levels (Table 2). At the system-wide level, the 976 ECFs generated 918 global Thiessen polygons after intersecting with the study region boundary, yielding a mean polygon area of 63.18 km^2, a standard deviation (SD) of 64.87 km^2, and a CV of 102.67%. This value far exceeds the conventional 64% threshold for clustered patterns, confirming that welfare ECFs are highly clustered across the entire region. Because the conventional 33–64% thresholds apply only to unclipped global Voronoi cells rather than administratively clipped subunit polygons, the subunit analysis focuses on the relative strength of spatial heterogeneity across hierarchical tiers rather than binary classification.

Table 2. Spatial characteristics of welfare ECF potential service areas across urban–rural hierarchical tiers.

Classification of ECF	Urban-Rural Structure Division (According to Administrative Level)	Number of Thiessen Polygons	SD (Area Size of Each Thiessen Polygon)	Average of Element Samples (Area Size of Each Thiessen Polygon)	CV Value	Spatial Characteristics (Structural Pattern)	VD Results
ECF (N = 976)		918	64,871,341.520 m^2	63,184,091.218 m^2	102.670%	Clustered	
Urban Districts (n = 23)		789	29,666,698.171 m^2	16,874,791.042 m^2	175.805%		
	Core Urban Districts (n = 15)	532	19,871,109.484 m^2	8,884,446.110 m^2	223.662%		
	Peripheral Urban Districts (n = 8)	257	38,455,925.782 m^2	33,415,115.960 m^2	115.085%		
County-Level Cities (n = 10)		336	62,573,975.197 m^2	57,582,293.624 m^2	108.669%		
	Directly Governed County-Level Cities (n = 3)	106	61,635,121.791 m^2	67,272,206.930 m^2	91.620%		
	General County-Level Cities (n = 7)	230	62,498,239.582 m^2	53,116,507.491 m^2	117.663%		
Rural Counties (n = 15)	Rural Counties (n = 15)	394	61,311,031.083 m^2	64,317,601.390 m^2	95.325%		

Note: Tier-level CV values are calculated from Thiessen polygon areas after spatial intersection with administrative boundaries. Higher CV indicates greater relative dispersion of potential service area fragments (i.e., stronger spatial heterogeneity). The large number of valid polygons across all tiers ($n > 100$) minimizes sampling error, ensuring that the observed CV variations are robust and attributable to structural spatial differences rather than random fluctuations.

Subunit-level analyses showed substantial variation in CV values across urban–rural administrative divisions. Urban districts exhibited the highest CV (175.81%; 789 clipped polygons). Within this tier, core urban districts showed the highest CV overall (223.66%; 532 polygons), whereas peripheral urban districts had a CV of 115.09% (257 polygons). County-level cities had a CV of 108.67% (336 polygons); directly governed county-level cities recorded a CV of 91.62% (106 polygons), while general county-level cities reached 117.66% (230 polygons). Rural counties had a CV of 95.33% (394 polygons).

Across all subunits, CV values ranged from 91.62% in directly governed county-level cities to 223.66% in core urban districts. These results indicate that the spatial fragmentation of welfare ECF potential service areas is most pronounced in core urban districts and least pronounced in directly governed county-level cities. The overall gradient confirms that urban districts—particularly core urban districts—exhibit substantially stronger internal heterogeneity in potential service area fragmentation than county-level cities and rural counties.

3.1.2. By Service Mode

The CV of Thiessen polygon areas revealed pronounced spatial heterogeneity for both institutional ECFs (IECFs) and community-based ECFs (CECFs) at both system-wide and subunit levels (Table 3). At the system-wide level, the 797 IECFs generated 766 Thiessen polygons (mean area: 75.72 km^2; SD: 65.80 km^2; CV: 86.90%), whereas the 179 CECFs generated 172 polygons (mean area: 337.23 km^2; SD: 629.47 km^2; CV: 186.66%). Both service modes exhibited CV values far exceeding the 64% threshold, confirming an overall clustered distribution under the unclipped global tessellation. As established, the subunit analysis focuses on relative heterogeneity across hierarchical tiers rather than binary classification.

At the subunit level, all divisions showed high CV values for both service modes. For IECFs, CV values ranged from 88.77% in directly governed county-level cities (102 polygons) to 195.78% in core urban districts (393 polygons). Urban districts exhibited a CV of 155.89% (629 polygons), while rural counties recorded 92.33% (376 polygons). For CECFs, CV values were consistently higher, ranging from 104.30% in directly governed county-level cities (17 polygons; interpret with caution due to small sample size) to 273.85% in core urban districts (220 polygons). Urban districts exhibited a CV of 242.09% (293 polygons), and rural counties recorded 140.73% (84 polygons).

CECFs had higher CV values than IECFs at both the system-wide level and in every subunit. The highest CV was observed for CECFs in core urban districts (273.85%), and the lowest for IECFs in directly governed county-level cities (88.77%). This pattern indicates that CECFs exhibit substantially greater spatial heterogeneity and fragmentation in their potential service areas than IECFs, a disparity that is most pronounced in core urban districts.

3.1.3. By Organizational Mode

The CV of Thiessen polygon areas differed markedly between organizational modes (Table 4). At the system-wide level, the 551 ECFs operated by government organization (GO) generated 541 polygons (mean area: 107.21 km^2; SD: 62.13 km^2; CV: 57.95%). This value falls within the 33–64% interval, conventionally indicating a random spatial structure. By contrast, the 425 ECFs operated by social organization (SO) generated 401 polygons (mean area: 144.65 km^2; SD: 344.30 km^2; CV: 238.03%), far exceeding the 64% threshold and indicating a highly clustered structure.

Table 3. Spatial characteristics of IECF and CECF potential service areas across urban–rural hierarchical tiers.

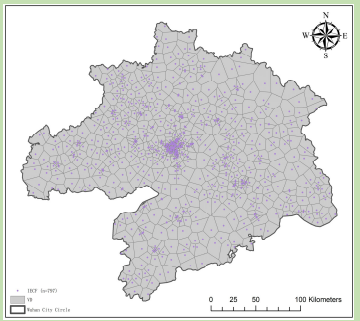
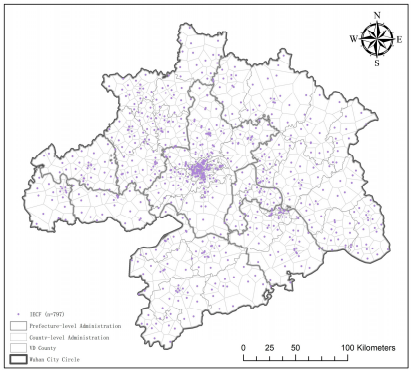
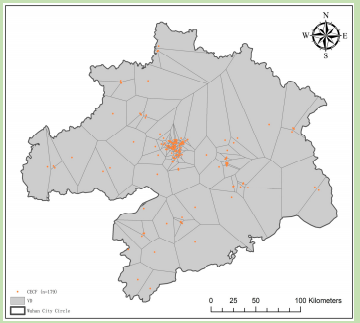
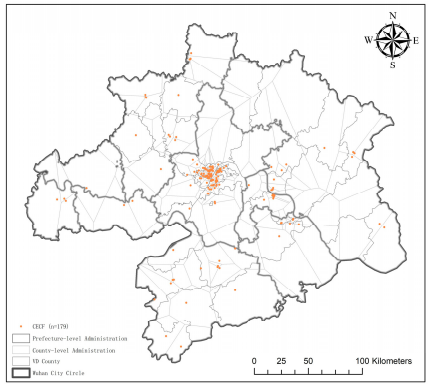
Classification of ECF	Urban-Rural Structure Division (According to Administrative Level)	Number of Thiessen Polygons	SD (Area Size of Each Thiessen Polygon)	Average of Element Samples (Area Size of Each Thiessen Polygon)	CV Value	Spatial Characteristics (Structural Pattern)	VD Results
IECF (N = 797)		766	65,804,452.018 m^2	75,721,926.552 m^2	86.903%	Clustered	
Urban Districts (n = 23)		629	32,996,922.362 m^2	21,167,265.713 m^2	155.887%		
	Core Urban Districts (n = 15)	393	23,546,077.936 m^2	12,026,782.014 m^2	195.780%		
	Peripheral Urban Districts (n = 8)	236	40,098,113.776 m^2	36,388,494.923 m^2	110.194%		
County-Level Cities (n = 10)		321	63,556,362.710 m^2	60,273,055.008 m^2	105.447%		
	Directly Governed County-Level Cities (n = 3)	102	62,056,432.421 m^2	69,910,332.693 m^2	88.766%		
	General County-Level Cities (n = 7)	219	63,747,617.396 m^2	55,784,459.922 m^2	114.275%		
Rural Counties (n = 15)	Rural Counties (n = 15)	376	62,227,198.934 m^2	67,396,635.499 m^2	92.330%		
CECF (N = 179)		172	629,471,348.681 m^2	337,226,719.410 m^2	186.661%	Clustered	

Table 3. *Cont.*

Classification of ECF	Urban-Rural Structure Division (According to Administrative Level)	Number of Thiessen Polygons	SD (Area Size of Each Thiessen Polygon)	Average of Element Samples (Area Size of Each Thiessen Polygon)	CV Value	Spatial Characteristics (Structural Pattern)	VD Results
Urban Districts (n = 23)		293	110,008,815.142 m^2	45,440,990.216 m^2	242.092%		
	Core Urban Districts (n = 15)	220	58,834,790.496 m^2	21,484,206.051 m^2	273.851%		
	Peripheral Urban Districts (n = 8)	73	176,633,093.506 m^2	117,639,517.834 m^2	150.148%		
County-Level Cities (n = 10)		63	429,213,838.574 m^2	307,105,565.994 m^2	139.761%		
	Directly Governed County-Level Cities (n = 3)	17	437,484,997.146 m^2	419,461,996.158 m^2	104.297%		
	General County-Level Cities (n = 7)	46	418,551,922.174 m^2	265,582,537.455 m^2	157.598%		
Rural Counties (n = 15)	Rural Counties (n = 15)	84	424,541,447.422 m^2	301,680,177.950 m^2	140.726%		

Note: Tier-level CV values are calculated from Thiessen polygon areas after spatial intersection with administrative boundaries. Higher CV indicates greater relative dispersion of potential service area fragments (i.e., stronger spatial heterogeneity). The large number of valid polygons across major tiers reduces sensitivity to small-count instability, supporting the interpretation that the observed CV variations reflect structural spatial differences rather than random fluctuations. Estimates derived from small sample subsets (e.g., specific county-level divisions) warrant cautious interpretation.

Table 4. Spatial characteristics of GO-operated and SO-operated ECF potential service areas across urban–rural hierarchical tiers.

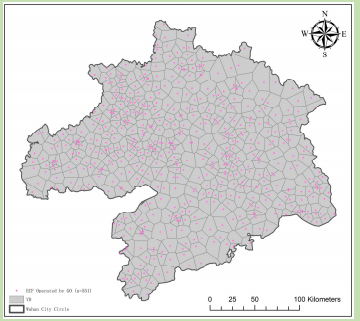
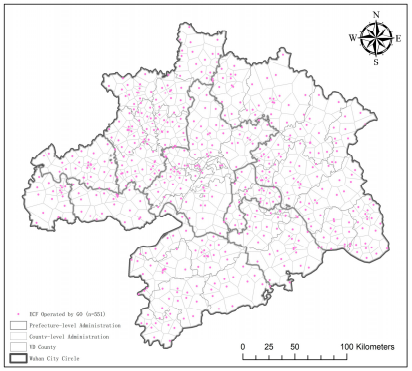
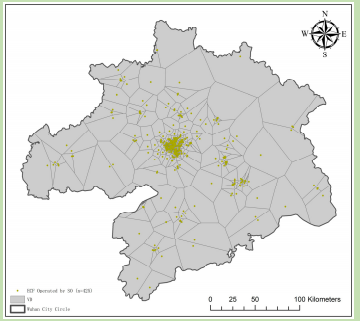
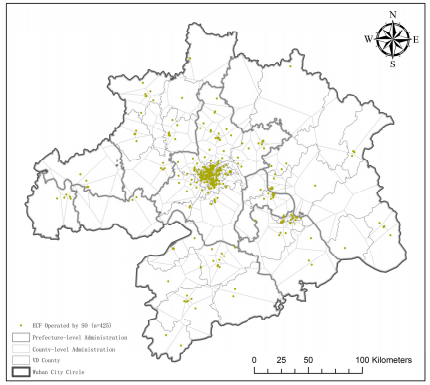
Classification of ECF	Urban-Rural Structure Division (According to Administrative Level)	Number of Thiessen Polygons	SD (Area Size of Each Thiessen Polygon)	Average of Element Samples (Area Size of Each Thiessen Polygon)	CV Value	Spatial Characteristics (Structural Pattern)	VD Results
ECF Operated by GO (N = 551)		541	62,125,606.586 m^2	107,214,409.868 m^2	57.945%	Random	
Urban Districts (n = 23)		324	45,077,653.252 m^2	41,093,241.152 m^2	109.696%		
	Core Urban Districts (n = 15)	158	35,297,791.413 m^2	29,914,717.287 m^2	117.995%		
	Peripheral Urban Districts (n = 8)	166	50,478,020.215 m^2	51,733,040.975 m^2	97.574%		
County-Level Cities (n = 10)		297	67,502,957.659 m^2	65,143,604.908 m^2	103.622%		
	Directly Governed County-Level Cities (n = 3)	98	62,346,279.853 m^2	72,763,815.660 m^2	85.683%		
	General County-Level Cities (n = 7)	199	69,596,830.750 m^2	61,390,938.306 m^2	113.367%		
Rural Counties (n = 15)	Rural Counties (n = 15)	359	64,003,165.878 m^2	70,588,119.632 m^2	90.671%		
ECF Operated by SO (N = 425)		401	344,296,181.338 m^2	144,645,874.660 m^2	238.027%	Clustered	

Table 4. *Cont.*

Classification of ECF	Urban-Rural Structure Division (According to Administrative Level)	Number of Thiessen Polygons	SD (Area Size of Each Thiessen Polygon)	Average of Element Samples (Area Size of Each Thiessen Polygon)	CV Value	Spatial Characteristics (Structural Pattern)	VD Results
Urban Districts (n = 23)		582	57,064,721.930 m^2	22,876,649.713 m^2	249.445%		
	Core Urban Districts (n = 15)	438	33,404,671.524 m^2	10,791,153.724 m^2	309.556%		
	Peripheral Urban Districts (n = 8)	144	89,283,463.821 m^2	59,636,700.013 m^2	149.712%		
County-Level Cities (n = 10)		95	355,771,111.800 m^2	203,659,480.607 m^2	174.689%		
	Directly Governed County-Level Cities (n = 3)	25	361,500,004.985 m^2	285,234,157.387 m^2	126.738%		
	General County-Level Cities (n = 7)	70	349,113,395.557 m^2	174,525,667.471 m^2	200.036%		
Rural Counties (n = 15)	Rural Counties (n = 15)	119	319,724,067.598 m^2	212,950,713.847 m^2	150.140%		

Note: Tier-level CV values are calculated from Thiessen polygon areas after spatial intersection with administrative boundaries. Higher CV indicates greater relative dispersion of potential service area fragments (i.e., stronger spatial heterogeneity). The large number of valid polygons across major tiers reduces sensitivity to small-count instability, supporting the interpretation that the observed CV variations reflect structural spatial differences rather than random fluctuations. Estimates derived from small sample subsets (e.g., specific county-level divisions) warrant cautious interpretation.

At the subunit level, CV values are compared directly across tiers to assess relative spatial heterogeneity. For GO-operated ECFs, CV values remained relatively stable and low across all divisions, ranging from 85.68% in directly governed county-level cities (98 polygons) to 118.00% in core urban districts (158 polygons). For SO-operated ECFs, CV values were substantially higher and more volatile, ranging from 126.74% in directly governed county-level cities (25 polygons; interpret with caution due to small sample size) to a striking 309.56% in core urban districts (438 polygons). Urban districts as a whole recorded a CV of 249.45% for SO-operated ECFs, compared to 109.70% for GO-operated ECFs.

Across all divisions, SO-operated ECFs had substantially higher CV values than GO-operated ECFs at both the system-wide level and in every subunit. The highest CV was observed for SO-operated ECFs in core urban districts (309.56%), and the lowest for GO-operated ECFs in directly governed county-level cities (85.68%). Thus, while GO-operated ECFs approached a random distribution at the macro scale, SO-operated ECFs exhibited severe clustering and fragmentation. This organizational divergence is most acute in core urban districts, indicating that social capital and market-driven eldercare resources are highly concentrated in urban centers, whereas government-led provisions maintain a more spatially dispersed baseline.

3.2. Locational Patterns: Localized High-Density Clusters

3.2.1. All Welfare ECFs and Classified by Service Mode or Organizational Mode

Multi-scale KDE reveals pronounced, scale-dependent variabilities in the spatial hotspots of ECFs across the WCC (Figure 5). Although the aggregated pattern of all ECFs is highly monocentric—with density peaks consistently anchored in Wuhan's metropolitan core—disaggregation by institutional type and governance mode uncovers markedly divergent spatial behaviors across scales.

At the micro-scale (10 km), all ECFs form a tightly bounded hotspot centered on the urban core, reflecting the entrenched concentration of welfare infrastructure and administrative capacity in Wuhan's central districts. By service mode, both IECFs and CECFs exhibit central clustering; however, this apparent spatial cohesion masks substantial internal divergence. When classified by organizational mode, SO-operated ECFs mirror this centralized pattern, whereas GO-operated ECFs form a mosaic of dispersed micro-hotspots, reflecting a jurisdiction-based allocation mechanism wherein every administrative tier establishes basic eldercare capacity within its own boundary.

At the meso-scale (20 km), density surfaces integrate across county boundaries, revealing broader spatial structure. The overall ECF distribution expands into a larger urban-core zone with weak secondary peaks, while category divergences become more pronounced. IECFs and CECFs converge into a single high-density nucleus, reinforcing their structural reliance on centralized systems. Meanwhile, GO-operated ECFs form a wide spatial footprint; their density hotspots notably diverge from the Wuhan metropolitan core, emerging across multiple peripheral regions (e.g., the northwestern WCC). This dispersed pattern is consistent with a jurisdiction-based allocation legacy, ensuring basic eldercare coverage across peripheral administrative tiers. By contrast, SO-operated ECFs remain highly clustered in the core.

At the macro-scale (30 km), KDE surfaces reveal the macroscopic welfare geography of the metropolitan region. All ECFs coalesce into a contiguous metropolitan-core dominance zone, illustrating the centripetal force of Wuhan's aging service ecosystem. Internal hierarchies persist, however. IECFs, CECFs, and SO-operated ECFs maintain the steepest density gradients, signifying entrenched centralization and institutional path dependence. In contrast, GO-operated ECFs display the most diffused macro-level distribution. With broad, low-intensity density surfaces, they constitute the only category that produces a regional-scale welfare scaffold capable of reaching peripheral counties.

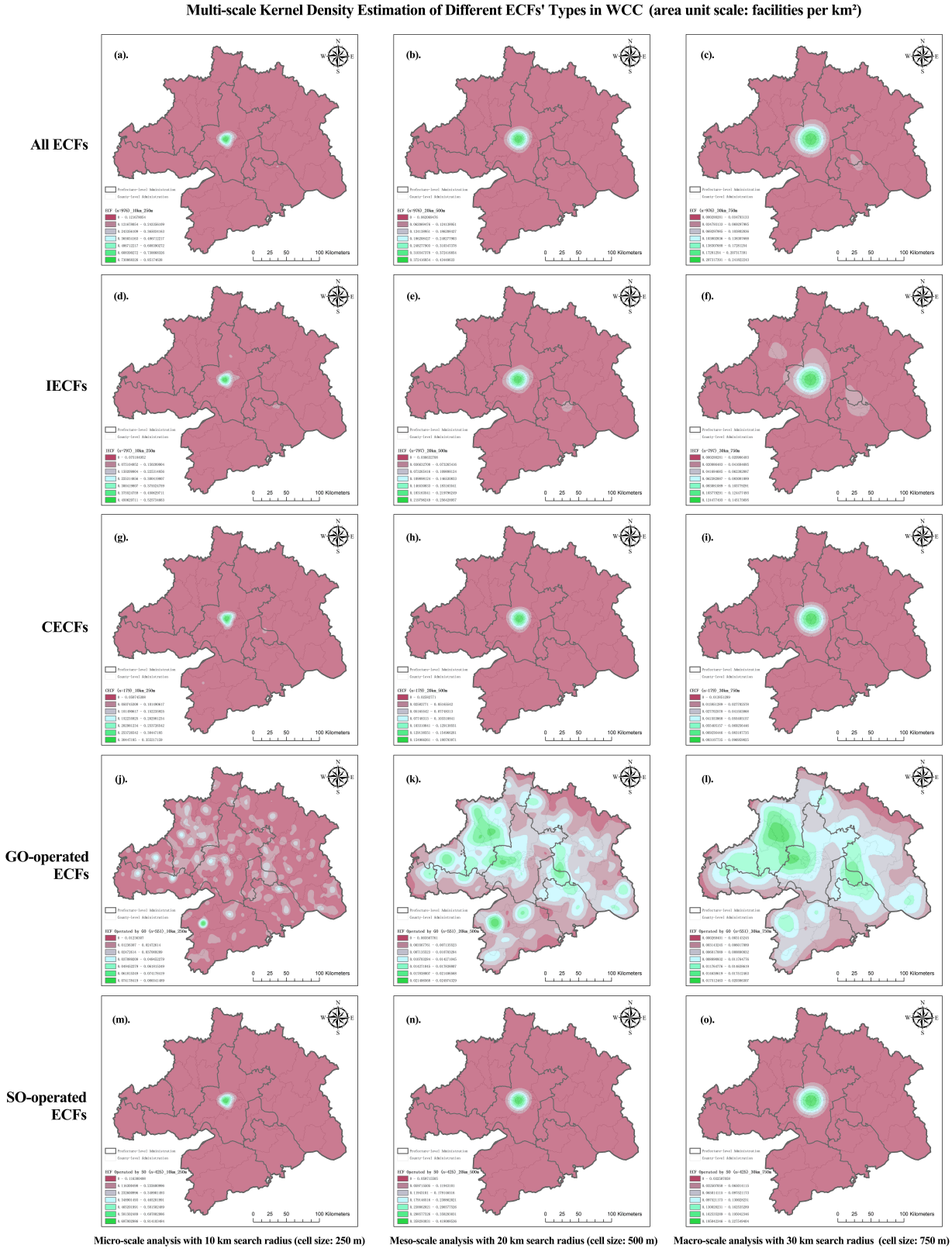


Figure 5. Spatial visualization of multi-scale KDE analysis of ECFs in WCC. The figure presents KDE results for all ECFs and their subtypes (classified by service mode: IECFs and CECFs; and organizational mode: GO-operated and SO-operated ECFs) at three scales; specifically, (**a**) all ECFs at the micro-scale (10 km search radius; 250 m cell size); (**b**) all ECFs at the meso-scale (20 km search radius; 500 m cell size); (**c**) all ECFs at the macro-scale (30 km search radius; 750 m cell size); (**d**) IECFs at the micro-scale (10 km search radius; 250 m cell size); (**e**) IECFs at the meso-scale (20 km

search radius; 500 m cell size); (**f**) IECFs at the macro-scale (30 km search radius; 750 m cell size); (**g**) CECFs at the micro-scale (10 km search radius; 250 m cell size); (**h**) CECFs at the meso-scale (20 km search radius; 500 m cell size); (**i**) CECFs at the macro-scale (30 km search radius; 750 m cell size); (**j**) GO-operated ECFs at the micro-scale (10 km search radius; 250 m cell size); (**k**) GO-operated ECFs at the meso-scale (20 km search radius; 500 m cell size); (**l**) GO-operated ECFs at the macro-scale (30 km search radius; 750 m cell size); (**m**) SO-operated ECFs at the micro-scale (10 km search radius; 250 m cell size); (**n**) SO-operated ECFs at the meso-scale (20 km search radius; 500 m cell size); and (**o**) SO-operated ECFs at the macro-scale (30 km search radius; 750 m cell size).

Across the three bandwidths, despite scale-dependent variations in local hotspot shapes, the overarching hotspot patterns remain broadly consistent. Specifically, the monocentric dominance of Wuhan, the core concentration of IECFs and CECFs, and the stark spatial divergence between GO-operated (peripheral scaffolding) and SO-operated (core concentration) ECFs are fundamentally robust. This cross-scale consistency can be interpreted as a bandwidth-sensitivity assessment, confirming that the observed core spatial structures are not mere artifacts of scale selection, but persistent features of the WCC's welfare geography.

3.2.2. All Welfare ECFs Classified by Function Type

Multi-scale KDE further reveals distinct spatial logics among different functional types, despite their operation within the same welfare regime (Figure 6). These disparities become increasingly structured as the analytical scale shifts from micro to macro.

At the micro-scale (10 km), elderly homes (EHs), elderly service centers (ESCs), and elderly service units (ESUs) exhibit highly localized concentration, anchored predominantly in the metropolitan core. This tight clustering reflects their dependence on existing institutional infrastructure. In contrast, elderly apartments (EAs) exhibit a multi-nodal pattern, with hotspots emerging both as high-end pilot projects within the primary core and as secondary clusters in suburban areas. This configuration indicates that EAs—as a less service-intensive but land-intensive model—tend to anchor in specific nodes that balance market demand with lower land acquisition and construction costs.

At the meso-scale (20 km), the density surfaces of all categories begin to coalesce, yet the degree of spatial convergence diverges sharply. EHs, ESCs, and ESUs remain a singular high-intensity cluster centered on Wuhan's inner metropolitan districts, underscoring their structural centralization. Meanwhile, EAs maintain a persistent multi-nodal structure, with high-end pilot projects anchored in the Wuhan core and experimental clusters extending to suburban and specific county-level areas (e.g., Huangshi urban districts and Huangpi).

At the macro-scale (30 km), KDE surfaces reveal the underlying metropolitan geography of welfare concentration. EHs, ESCs, and ESUs remain core-centric surfaces, reinforcing a structurally centralized elderly-care ecosystem with diminishing service intensity toward the periphery. However, EAs retain a multi-nodal spatial configuration even at this scale, highlighting their unique role as a transitional model that bridges high-end services in the primary core with experimental demand in peripheral and secondary-city cores.

Across the three bandwidths, despite scale-dependent variations in local hotspot shapes, the overarching hotspot patterns remain broadly consistent. Specifically, the central clustering of EHs, ESCs, and ESUs, alongside the multi-nodal anchoring of EAs, is fundamentally robust. This cross-scale consistency can be interpreted as a bandwidth-sensitivity assessment, confirming that the identified spatial mismatch between care intensity and locational costs is not a mere artifact of scale selection, but a persistent structural reality of the WCC's welfare geography.

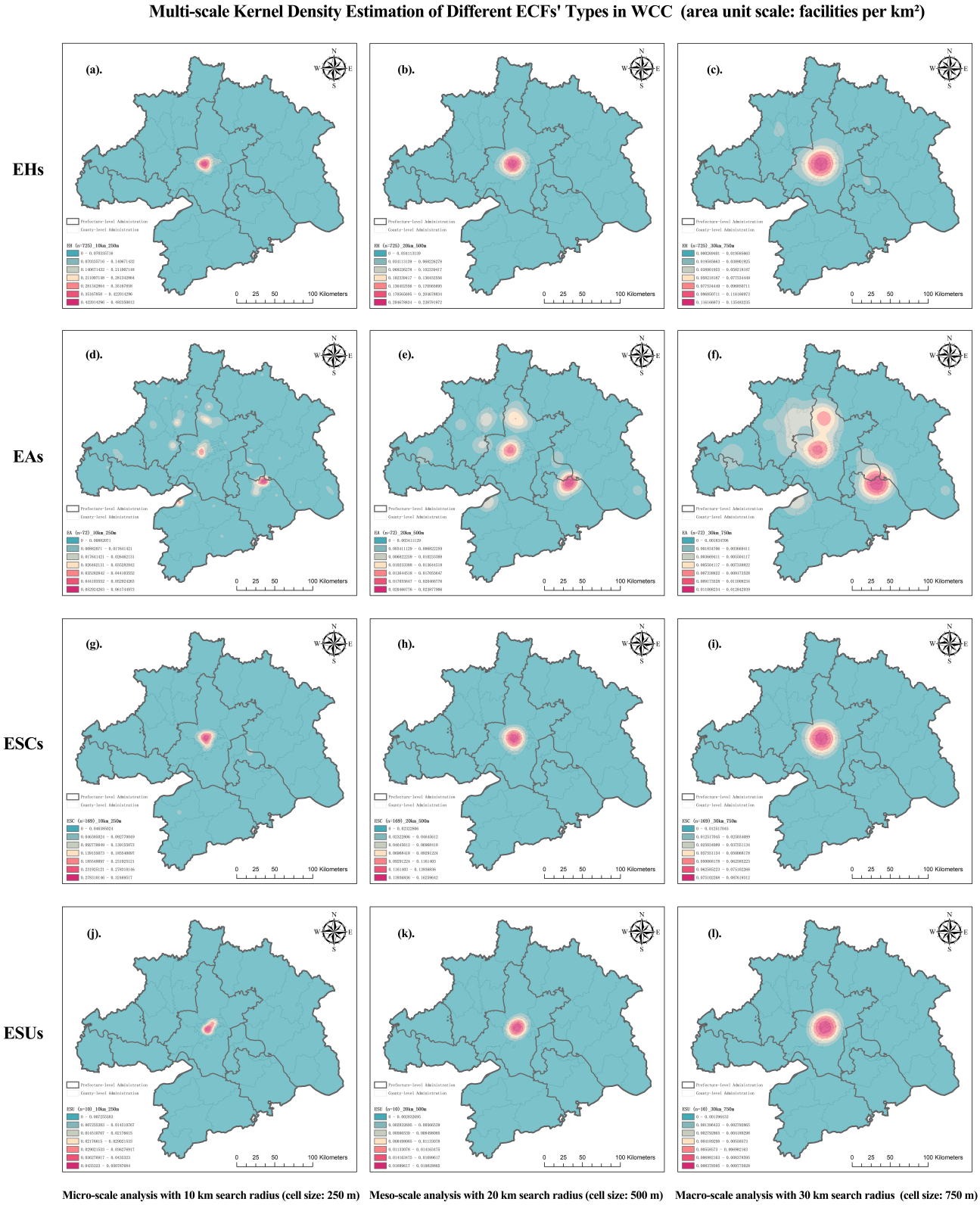


Figure 6. Multi-scale KDE of different ECF types in WCC. The figure presents KDE results for different ECF types (EHs, EAs, ESCs, and ESUs) at three scales; specifically, (**a**) EHs at the micro-scale (10 km search radius; 250 m cell size); (**b**) EHs at the meso-scale (20 km search radius; 500 m cell size); (**c**) EHs at the macro-scale (30 km search radius; 750 m cell size); (**d**) EAs at the micro-scale (10 km search radius; 250 m cell size); (**e**) EAs at the meso-scale (20 km search radius; 500 m cell size); (**f**) EAs at the macro-scale (30 km search radius; 750 m cell size); (**g**) ESCs at the micro-scale (10 km

search radius; 250 m cell size); (**h**) ESCs at the meso-scale (20 km search radius; 500 m cell size); (**i**) ESCs at the macro-scale (30 km search radius; 750 m cell size); (**j**) ESUs at the micro-scale (10 km search radius; 250 m cell size); (**k**) ESUs at the meso-scale (20 km search radius; 500 m cell size); and (**l**) ESUs at the macro-scale (30 km search radius; 750 m cell size).

4. Discussion

4.1. Spatial Organization and Differentiation of Eldercare Provision in the WCC

4.1.1. Deconstructing the Monocentric Collapse: Internal Fragmentation and Core Dominance

The diagnostic value of the clipped-Voronoi CV lies in reframing the unit of analysis: rather than asking how many facilities a district contains or how far the nearest facility lies, it asks how unevenly potential service areas are distributed among facilities once administrative boundaries are imposed. High CV in core urban districts therefore signifies not simply density but an extreme internal polarization: a few facilities absorb vast potential service areas while many others are compressed into narrow geometric fragments—a structural condition invisible to aggregate supply counts. This internal fragmentation, measured at CV = 223.66% in core urban districts against a system-wide 102.67% across all ECFs, constitutes the empirical signature of what is termed here a "monocentric collapse". KDE surfaces corroborate this structure at every scale: both aggregated and disaggregated peaks anchor overwhelmingly in Wuhan's inner metropolitan districts, while density gradients decay monotonically toward peripheral counties. Consequently, high-quality institutional eldercare is locked into a single gravitational center, undermining the regional sustainability of the welfare healthy landscape by concentrating geometric service networks in land-scarce cores while leaving peripheral counties with sparse and large potential service areas. Notably, the lower CV in rural counties (95.33%) does not indicate sufficiency; rather, it reveals structural marginality—characterized by limited fiscal capacity, constrained professional labor, and only a few ECF nodes dispersed across vast administrative territories.

This polarization acquires theoretical significance when situated within the political economy of the Wuhan City Circle. Wuhan's primacy is not merely a matter of economic scale; rather, it represents a profound spatial polarization that concentrates the overwhelming share of regional competitiveness and higher-order public resources [49,70,71]. It exhibits the spatial logic Brenner terms state spatial selectivity—the privileging of particular territories through the unequal allocation of administrative capacity, fiscal investment, and policy attention, thereby shaping the geographies of uneven development [72–74]. The finding that core urban districts exhibit the highest service-area heterogeneity is therefore not merely a product of a hierarchical state spatial process. Instead, it signifies that metropolitan primacy functions as a fertile ground for welfare reproduction: the core's superior infrastructure and institutional thickness readily accommodate and attract eldercare provisions, creating extreme spatial competition and geometric fragmentation.

Furthermore, this structural reading challenges the prevailing policy emphasis on aggregate supply targets and the urban–rural binary [10,11,19]. While regional inequality is well documented [14,20–24], the multi-scale diagnostic shows that the sharpest spatial divergence lies not merely between urban and rural areas, but within the urban core itself. Recent studies in Kunming have documented a similar "primary core-multiple satellite" structure, with public service resources highly concentrated in central districts [75]. However, the WCC's core CV of 223.66%, contrasting with peripheral county values of 91.62–117.66%, indicates that "monocentric" here denotes not a benign center–hinterland hierarchy, but a strong fragmentation internal to the center. Evidence from Beijing corroborates this mechanism: service-type community facilities exhibit an overlap rate of 199.32% within 15-min walking catchments, indicating intense localized competition and redundant deployment

in core districts, whereas residential-type facilities reach only 15.84% coverage in outer districts [76]. Evidence from Dalian likewise identifies a spatial-equity deficit characterized by oversupplied urban cores and underserved peripheries, with recommended reallocation from central to peripheral districts [77]. Thus, core over-agglomeration and peripheral sparse coverage are not two independent problems, but two spatial expressions of the same underlying logic.

4.1.2. Institutional Divergence: Administrative Scaffolding Versus Market Selectivity

The organizational divide reveals two entirely distinct spatial logics operating within a single welfare regime. GO-operated ECFs approximate a random-like, dispersed distribution (system-wide CV = 57.95%), whereas SO-operated ECFs exhibit extreme core concentration (CV = 238.03%). Multi-scale KDE surfaces further corroborate this bifurcation: SO-operated ECFs remain rigidly anchored in the monocentric core, whereas GO-operated ECFs manifest as a dispersed mosaic of micro-hotspots extending into peripheral regions. This spatial divergence—extreme core concentration versus peripheral dispersion—represents a fundamental institutional contrast rather than a mere difference in degree.

The core concentration of SO-operated ECFs reflects a distinct spatial selectivity of organizations; even when operating under a non-profit mandate, these entities are notably drawn to locations with superior institutional environments, infrastructure, and market conditions [47,78–81]. While the present spatial data do not directly measure demand or purchasing power, this pattern aligns with the documented locational logic of social eldercare providers in China—including the "economic paradox" where facility locations tend to follow retirees' disposable income, while high land values in prosperous cores crowd out land-intensive facilities [82]. By contrast, the dispersed GO pattern is not a deliberate market-correcting instrument, but a spatial legacy of an early-established, jurisdiction-based welfare framework. Historical institutionalist accounts of Chinese welfare demonstrate strong path dependence, wherein planned-economy legacies such as the work-unit system and household registration continue to structure welfare provision [83]. This reflects that long before the substantial entry of social forces into the eldercare sector, the government had already established a basic welfare coverage logic rooted in administrative hierarchies and jurisdictional boundaries. Consistent with this, the spatial data reveal that many GO-operated ECFs were registered in earlier periods, operationalizing this administrative coverage logic before market competition intensified. Furthermore, the more spatially even deployment in directly governed county-level cities suggests a moderating effect of administrative autonomy, albeit potentially confounded by the more regular geometries of their finer-grained administrative boundaries.

This bifurcation corroborates critical perspectives on welfare governance [33,34]. The political economy of aging literature reveals how pervasive profit motivations and capital switching penetrate institutional boundaries, even across nominal state and not-for-profit divides [81]. This raises the concern that the extreme core concentration of social providers may reflect a structural susceptibility to market forces rather than purely altruistic welfare delivery, a dynamic that ultimately (re)produces spatial inequalities in provision [81,84]. The historically embedded GO-operated ECFs, by contrast, function as spatial equalizers. Ultimately, this structural mismatch reveals the spatial dilemma of welfare pluralism. The mixed economy of care can produce unequalizing outcomes in access when different providers operate under divergent spatial logics [85]. In the Chinese context, although non-governmental investment can theoretically exert a positive effect on regional equalization, this effect is often inhibited by multiple factors, including government investment crowding-out and spatial misallocation [86], the sensitivity of private eldercare investment to local demand density rather than policy-directed spatial allocation [87], the "siphon effect" of

capital and skilled care labor toward core cities [82], and regional imbalances in market mechanism maturity that constrain social capital participation in peripheral areas [88]. The WCC evidence demonstrates that relying solely on the actual spatial configuration of SO not only fails to achieve spatial parity but actively exacerbates regional polarization. This finding challenges the prevailing narrative that welfare pluralism alone can achieve the "Equalization of Basic Public Services" [42–44,47], suggesting that a mere expansion of social providers does not inherently translate into a geographically balanced provision.

4.1.3. Functional Differentiation: Divergent Spatial Logics of Eldercare Typologies

Beyond institutional modes, functional types reveal a spatial mismatch between care intensity and locational costs. While all high-intensity facilities—EHs, ESCs, and ESUs—share a strong central gravitational pull toward Wuhan [35], their spatial footprints differ fundamentally. EAs exhibit a selective central anchoring configuration at varying spatial scales. Rather than diffusing uniformly, EAs strategically anchor in specific regional nodes—ranging from the Wuhan core as high-end pilot projects, to peripheral urban districts like Huangpi, and to the core urban districts of secondary cities like Huangshi—a pattern in which operating-cost pressures may play an important role [82]. This multi-nodal extension relieves spatial pressure in the Wuhan core, creating a decentralized landscape that contrasts with the localized clustering of ESUs.

This functional gradient also mirrors the spatial divergence between baseline provision and innovative models. While EHs generate high-density hotspots in the urban core, their overall spatial data footprint reveals a wide-reaching spatial skeleton. They form the stable baseline of institutional care, providing cross-district capacity for basic needs. In contrast, innovative models like EAs and ESUs—largely operated by social forces—exhibit highly localized, experimental clustering. Constrained by external resource dependencies, these facilities struggle to form coherent service corridors at the community or county scales. Instead, EAs form partially polycentric hotspot structures—neither fully embedded in traditional cores nor evenly dispersed. This pattern can be interpreted as a configuration of strategic testing nodes: facilities are deployed at selected locations to trial new service models, yet the risk remains that they evolve into isolated service enclaves rather than functioning as bridges between core and peripheral areas.

Despite these functional mismatches and the risk of spatial fragmentation, the spatial distribution of the WCC's ECFs reveals a systematic service hierarchy characterized by "institutional diffusion—community anchoring—site-level penetration" (Figure 7):

- **EHs—Wide Diffusion:** EHs exhibit the broadest geographic reach and cross-district service capacity (notwithstanding their concentrated core hotspots), forming the foundational layer of institutional care provision.
- **EAs—Selective Central Anchoring:** EAs emerge as a spatially selective, node-anchored facility type. Rather than diffusing into rural villages or scattered neighborhoods, their spatial footprint is strategically limited to established urban nodes—such as central Wuhan, peripheral districts (e.g., Huangpi), and regional city cores (e.g., Huangshi)—functioning as a high-specialization supplement to the widely diffused EH system.
- **ESCs—Meso-scale Radiation**: ESCs display meso-scale regional radiation, forming dense community-level clusters that support local aging-in-place services.
- **ESUs—Point-based Penetration**: ESUs appear as highly localized, point-based support nodes, extending and refining the community-scale ESC network.

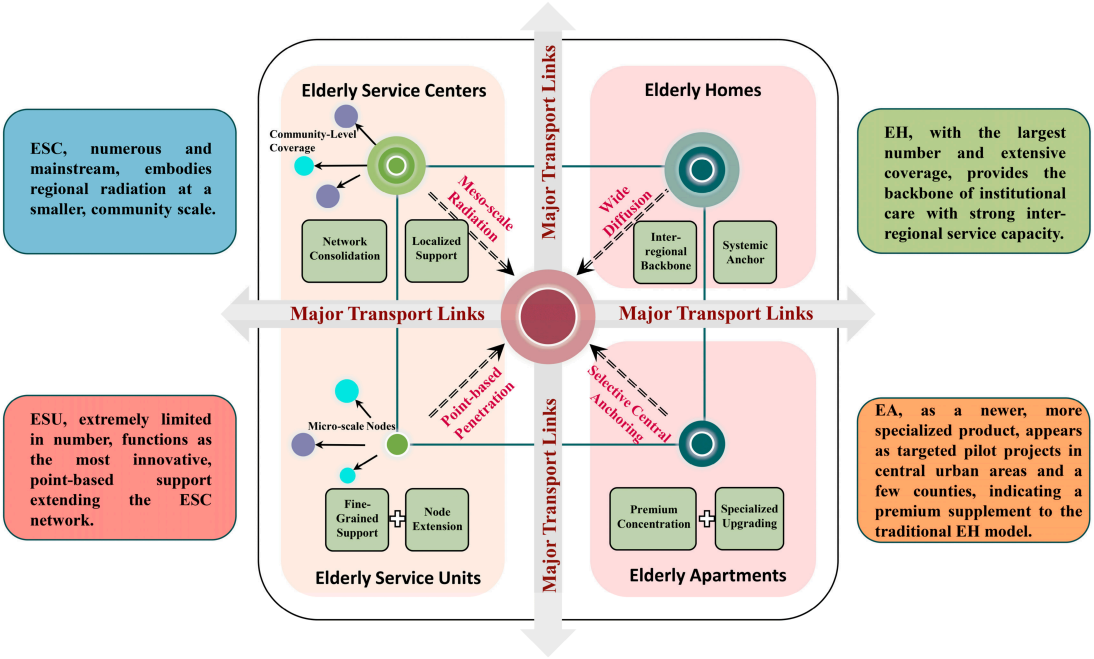


Figure 7. Typological synthesis of spatial logics across welfare ECF functional types in the WCC.

4.2. Policy Implications: Targeted Spatial Interventions for Welfare Landscapes

The diagnostic evidence from the WCC carries a clear policy message: spatial inequality in eldercare is not a residual planning failure to be resolved through aggregate capacity expansion, but a structural outcome of divergent institutional logics interacting within a hierarchically organized territorial system. Policies that continue to prioritize total bed counts or the urban–rural binary will leave the mechanisms that produce spatial polarization intact. What is required is a shift from supply-side expansion to spatially targeted intervention.

4.2.1. Spatial Steering of Market-Driven Provision: From Unqualified Expansion to Location-Sensitive Incentives

The extreme core concentration of SO-operated ECFs and the documented "siphon effect" of capital and skilled care labor toward core cities [82] indicate that unleashing market forces without spatial governance will intensify, not mitigate, polarization. Because a one-size-fits-all policy of "encouraging social participation" may inadvertently reinforce this inequality, governance must be differentiated by organizational mode. Spatial steering instruments should move beyond demand-side subsidies toward location-sensitive incentives. Recent evidence recommends combining restrictive zoning in saturated cores with targeted subsidies in underserved peripheries [76], and calls for targeted cost-offset subsidies in high-tier cities as necessary complements to aggregate supply targets [82]. Spatial optimization research from Dalian suggests that reallocating beds from oversupplied urban cores to underserved peripheries is a feasible strategy to enhance spatial equity [77]. Extending this spatial logic to the regional scale of the WCC, policy interventions should prioritize location-sensitive incentives—such as cross-jurisdictional subsidy transfers—to steer market-driven SO-operated ECFs away from Wuhan's saturated core and toward underserved peripheral nodes.

4.2.2. A Public Baseline for Peripheral Counties: The Three-Tier Network as Structural Remedy

The finding that rural counties exhibit lower CV does not indicate spatial equity, but rather reflects absolute sparsity. In vast rural territories, a limited number of facilities

inherently creates large, similarly sized service areas, generating a geometric illusion of balance while masking substantive deprivation. Against this backdrop of sparse and disconnected nodes, GO-operated ECFs serve as the only reliable anchor. Policy should therefore reinforce their baseline role in guaranteeing basic provision across peripheral jurisdictions, rather than subjecting them to market competition. In the Chinese context, this implies constructing a three-tier service network: a county-level hub for resource coordination, township-level centers as intermediate nodes, and village-level stations for last-mile access [89,90]. The stated objective of this national plan is precisely to "integrate fragmented care resources into a three-tier system that extends from urban centers to remote rural communities" [89,90]. Ultimately, such a hierarchical network serves as a structural remedy, replacing sparse, disconnected nodes with interconnected coverage to address the substantive deficit.

4.2.3. Functionally Differentiated Planning Standards: Replacing Universal Benchmarks with Type-Specific Spatial Rules

EHs, ESCs, and ESUs exhibit central clustering driven by their operational dependencies, whereas EAs anchor in selected urban nodes at varying scales. A single density target or per-capita bed ratio cannot accommodate this heterogeneity. Particularly for CECFs, which exhibit severe spatial fragmentation, the policy response should move from a narrow focus on per-capita construction standards to a networked stitching approach. Evidence from high-density cities demonstrates a stark paradox: while core districts suffer from redundant deployment (e.g., overlapping service radii), peripheral areas face severe care blind spots [76]. Therefore, rather than blindly expanding the 15-min service circle, dynamic and fine-grained supply–demand matching [47,91] should be utilized to reconcile this imbalance. For saturated cores and highly fragmented older districts [92], instead of difficult physical consolidation, policies should promote networked chain operations and shared service platforms to de-densify overlapping catchments. Conversely, in underserved peripheral gaps, targeted spatial infill must be prioritized to extend basic coverage. By coupling the de-densification of oversupplied zones with the reinforcement of blind spots, the eldercare network can transition from fragmented embedding to coherent regional coverage.

4.2.4. Cross-Jurisdictional Coordination: Addressing Spatial Inequality as a Regional Rather than Local Problem

The WCC's monocentric structure means that the spatial reach of core-city facilities and the service deficits of peripheral counties are not separate jurisdictional problems but expressions of a single regional welfare geography. Within core urban districts, the highest spatial heterogeneity suggests that policy priorities should shift from density expansion to structural rebalancing—using spatial diagnostics to identify oversized fragments and prioritizing targeted infill in these coverage blind spots. At the regional scale, the siphon effect identified in the spatial spillover literature requires "a shift from localized planning to regional coordination", with local governments establishing cross-regional elderly care consortia and creating shared resource pools and mutual recognition of elderly care subsidies across city borders [82]. Without such coordination, individual jurisdictions will continue to optimize within their own boundaries while collectively reproducing the regional polarization that the diagnostic evidence has identified.

4.3. Limitations and Future Research Directions

As an ESDA, this study primarily aims to identify spatial patterns and generate hypotheses rather than establish causal mechanisms. Several limitations should be acknowledged:

the cross-sectional design captures the spatial distribution of ECFs at a specific point in time, limiting its ability to reveal temporal changes; the absence of demand- and capacity-related variables constrains the assessment of whether the observed distribution translates into actual service adequacy and coverage; the reliance on Euclidean distance captures spatial proximity but does not account for physical barriers or actual transport conditions; and administrative boundary effects alongside scale sensitivity may influence the measured spatial patterns and their interpretation.

These limitations preclude definitive causal conclusions but do not diminish the empirical value of the observed spatial structures. Rather, the interpretations are firmly grounded in spatial evidence and engagement with the existing literature, and should be understood as highly plausible, evidence-informed hypotheses rather than final causal claims. To overcome these constraints, four macro-level directions emerge for future research:

(1) **Multivariate integration and forecasting:** Integrating broader structural factors (e.g., socio-economic development, demographic shifts, local governance factors, and detailed policies) alongside fine-grained demand forecasting to evaluate long-term dynamic spatial equity.
(2) **Mechanism explanation and causal inference:** Transitioning from exploratory spatial pattern detection to rigorous mechanism validation, establishing robust causal links between institutional logics and spatial outcomes.
(3) **Longitudinal and multi-stakeholder dynamics:** Tracking the dynamic evolution of welfare landscapes to assess whether public provisions can persistently resist market-driven polarization over time.
(4) **Global comparative analysis:** Extending this framework to other aging regions (especially in Europe and Asia) to determine which spatial patterns are universal features of aging societies and which are contingent upon specific institutional regimes.

5. Conclusions

This study advances a structural–locational nexus based on ESDA to examine how spatial imbalances in welfare ECFs are produced and organized within the WCC, a monocentric metropolitan region with a wide urban–rural development gradient. Moving beyond descriptive mapping and technical-efficiency framing, the analysis conceptualizes spatial inequality as a structural outcome embedded in hierarchical service systems and territorial governance. Three principal findings emerge:

- The observed ECF distribution reveals a spatial imbalance that is not merely an incidental byproduct of uneven growth, but a persistent structural pattern. The evidence demonstrates that spatial polarization is defined not merely by urban–rural disparities, but by severe internal fragmentation within the urban core, which coexists with structural marginality in vast, sparsely covered peripheral counties.
- This spatial polarization appears to be structured by institutional divergence. Market-oriented social organizations exhibit pronounced spatial selectivity, concentrating disproportionately in more profitable core areas despite their non-profit mandates. In contrast, historically embedded GO-operated ECFs function as a decentralized administrative scaffolding, serving as the only reliable spatial anchor to guarantee basic coverage in peripheral regions.
- Functional differentiation reveals a distinct spatial hierarchy within this institutional landscape. High-intensity facilities (EHs, ESCs, and ESUs) remain heavily clustered in the primary center, whereas EAs selectively anchor across established primary and sub-centers.

Together, these findings demonstrate that spatial imbalance in eldercare provision is not an incidental planning failure but a systemic feature of territorial governance, reflecting and reinforcing core–periphery inequalities within China's metropolitan economies. For welfare landscapes to be sustainable under rapid population aging, interventions must shift from aggregate supply targets to spatially targeted restructuring. This necessitates a multilevel governance framework: spatially steering market forces toward underserved peripheries; implementing functionally differentiated planning standards to replace universal benchmarks with dynamic supply–demand matching; reinforcing a three-tier public network to remedy rural structural deficits; and establishing cross-jurisdictional coordination mechanisms to dismantle the boundary constraints of administrative localism. Ultimately, as China approaches its demographic aging peak, achieving spatial parity in eldercare requires moving beyond conventional metrics to embrace scale-sensitive, structurally informed diagnostics that explicitly address geographical distributional imbalances within the architecture of welfare governance.

Author Contributions: Conceptualization, J.X.; methodology, J.X.; software, J.X.; validation, J.X. and W.L.; formal analysis, J.X.; investigation, J.X., W.L. and H.Z.; resources, J.X., W.L., H.Z., N.H.H.L. and C.S.F.; data curation, J.X. and W.L.; writing—original draft preparation, J.X.; writing—review and editing, J.X., W.L., H.Z., N.H.H.L. and C.S.F.; visualization, J.X.; supervision, N.H.H.L. and C.S.F.; project administration, J.X., N.H.H.L. and C.S.F.; funding acquisition, J.X. All authors have read and agreed to the published version of the manuscript.

Funding: This research received no external funding.

Institutional Review Board Statement: Not applicable.

Informed Consent Statement: Not applicable.

Data Availability Statement: The original contributions presented in this study are included in the article. Further inquiries can be directed to the corresponding author upon reasonable request, subject to privacy, legal, and ethical restrictions.

Acknowledgments: We thank the four anonymous reviewers for their thoughtful comments, which improved the clarity and quality of this manuscript. During the preparation of this manuscript, the authors used DeepSeek-V4 and Grammarly for Windows (V1.2) to assist with grammar checking, synonym selection, and sentence-flow improvement, thereby enhancing readability. After using these tools/services, the authors reviewed and edited the content as needed and took full responsibility for the content of the manuscript.

Conflicts of Interest: The authors declare no conflict of interest.

Abbreviations

ANN	Average Nearest Neighbor
API	Application Programming Interface
CECFs	Community-Based ECFs
CV	Coefficient of Variation
EAs	Elderly Apartments
ECFs	Elderly Care Facilities
EHs	Elderly Homes
ESCs	Elderly Service Centers
ESDA	Exploratory Spatial Data Analysis
ESUs	Elderly Service Units
GO	Government Organization
IECFs	Institutional ECFs
KDE	Kernel Density Estimation
SD	Standard Deviation

SO	Social Organization
UN	United Nations
UTM	Universal Transverse Mercator
WCC	Wuhan City Circle
WGS 1984	World Geodetic System 1984
VD	Voronoi Diagram

References

1. Yap, W.; Duarte, F.; Zheng, Y.; Jang, K.M.; Luo, P.; Vineis, P.; Ratti, C.; Biljecki, F. Urban motifs associated with population health. *Nat. Health* **2026**, *1*, 283–1298. [CrossRef]
2. Dou, H.; Wang, C.; Cheng, G.; Lei, X.; Xu, S. The vision of younger-seniors-based elderly care in rural China: Based on population aging predictions from 2020 to 2050. *Humanit. Soc. Sci. Commun.* **2025**, *12*, 669. [CrossRef]
3. Wen, F.; Liu, Z.; Zhang, B.; Zhang, Y.; Zhang, Z.; Zhang, Y. A Machine Learning-Based Study on the Demand for Community Elderly Care Services in Central Urban Areas of Major Chinese Cities. *Appl. Sci.* **2025**, *15*, 4141. [CrossRef]
4. Jiang, H.; Guo, Z.; Zhang, Y.; Zhang, H. Progressive Relationship Between Sustainable Development of Elderly Care Institutions and Spatial Environmental Factors: A Study Based on the Influence of Supermarkets, Medical Accessibility, and Parks in Urban Areas. *Risk Manag. Healthc. Policy* **2023**, *16*, 2037–2049. [CrossRef] [PubMed]
5. Cui, X.; Ma, L.; Tao, T.; Zhang, W. Do the supply of and demand for rural public service facilities match? Assessment based on the perspective of rural residents. *Sustain. Cities Soc.* **2022**, *82*, 103905. [CrossRef]
6. Guida, C.; Carpentieri, G.; Masoumi, H. Measuring spatial accessibility to urban services for older adults: An application to healthcare facilities in Milan. *Eur. Transp. Res. Rev.* **2022**, *14*, 23. [CrossRef] [PubMed]
7. Feng, Q.Q.; Ao, Y.B.; Chen, S.Z.; Martek, I. Evaluation of the allocation efficiency of medical and health resources in China's rural three-tier healthcare system. *Public Health* **2023**, *218*, 39–44. [CrossRef] [PubMed]
8. Li, X.; Zhu, J.; Wan, J.; Wang, Z. Equilibrium in adversity: Balancing public service supply and demand during population decline. *Humanit. Soc. Sci. Commun.* **2024**, *11*, 1760. [CrossRef]
9. Hai, L.; Cui, Y.; Zhang, J.; Wang, R. The dynamic equilibrium between population aging and the allocation of elderly medical care resources in the Yellow River Basin. *BMC Public Health* **2025**, *25*, 2510. [CrossRef] [PubMed]
10. Feng, Z.; Liu, C.; Guan, X.; Mor, V. China's Rapidly Aging Population Creates Policy Challenges in Shaping a Viable Long-Term Care System. *Health Aff.* **2012**, *31*, 2764–2773. [CrossRef] [PubMed]
11. Sehatkarlangrodi, S.; Zargoush, M.; Longo, C.J.; Ghazalbash, S. Shaping older adults' care policy: A scoping review of key determinants in post-acute and community reintegration transitions. *BMC Health Serv. Res.* **2025**, *25*, 1236. [CrossRef] [PubMed]
12. Li, M.; Ao, Y.; Deng, S.; Peng, P.; Chen, S.; Wang, T.; Martek, I.; Bahmani, H. A Scoping Literature Review of Rural Institutional Elder Care. *Int. J. Environ. Res. Public Health* **2022**, *19*, 10319. [CrossRef] [PubMed]
13. Jiang, Z.; Wu, C.; Chung, H. The 15-minute community life circle for older people: Walkability measurement based on service accessibility and street-level built environment—A case study of Suzhou, China. *Cities* **2025**, *157*, 105587. [CrossRef]
14. Wan, D.; Liu, H.; Guo, J.; Guo, L.; Qi, D.; Zhang, S.; Li, P.; Fukuda, H. Spatial Distribution and Accessibility Measurements for Elderly Day Care Centers in China's Urban Built-up Area: The Case of Tianjin Nankai District. *Buildings* **2022**, *12*, 1413. [CrossRef]
15. Wei, L.; Fang, Y.; Zhang, L. Identifying Accessibility and Equity Defects of Elderly Care Services in Developing Countries: Insights from Xiamen City. *J. Nurs. Manag.* **2024**, *2024*, 9340456. [CrossRef] [PubMed]
16. Jin, M.; Deng, Q.; Wang, S.; Wei, L. Equity Evaluation of Elderly-Care Institutions Based on Ga2SFCA: The Case Study of Jinan, China. *Sustainability* **2023**, *15*, 16943. [CrossRef]
17. Li, M.; Peng, P.; Zhu, H.; Ao, Y.; Zhou, Z. Exploring the equitable spatial planning on the accessibility of institutional elderly care in megacity: A study based on Chengdu, China. *Sustain. Cities Soc.* **2024**, *117*, 105998. [CrossRef]
18. Zhang, J.; Chen, Y.; Hu, Y.; Lai, L. Spatial Equality of Urban Care Facilities from the Perspective of Refinement: An Example from Changchun, China. *Land* **2023**, *12*, 1676. [CrossRef]
19. Yu, Y.; Dong, T. Deep Learning-Driven Geospatial Modeling of Elderly Care Accessibility: Disparities Across the Urban-Rural Continuum in Central China. *Appl. Sci.* **2025**, *15*, 4601. [CrossRef]
20. Li, X.; Li, C.; Huang, Y. Spatial-temporal analysis of urban-rural differences in the development of elderly care institutions in China. *Front. Public Health* **2022**, *10*, 1086388. [CrossRef] [PubMed]
21. Chen, X.; Chen, B.; Zhang, H.; Wong, C.U.I. Research on the Spatial and Temporal Distribution Evolution and Sustainable Development Mechanism of Smart Health and Elderly Care Demonstration Bases Based on GIS. *Appl. Sci.* **2024**, *14*, 780. [CrossRef]
22. Li, M.; Ao, Y.; Peng, P.; Bahmani, H.; Han, L.; Zhou, Z.; Li, Q. Resource allocation of rural institutional elderly care in China's new era: Spatial-temporal differences and adaptation development. *Public Health* **2023**, *223*, 7–14. [CrossRef] [PubMed]

23. Zheng, T.; Ma, X.; Cheng, X. Spatial pattern and influencing factors of urban elderly meal assistance facilities: A case study from Beijing, China, based on multi-source data. *J. Asian Archit. Build. Eng.* **2026**, *25*, 5072–5089. [CrossRef]
24. Li, C.; Wu, J.; Huang, Y. Spatial-Temporal Patterns and Coupling Characteristics of Rural Elderly Care Institutions in China: Sustainable Human Settlements Perspective. *Sustainability* **2023**, *15*, 3286. [CrossRef]
25. Bao, M.; Ma, R.; Chao, J. Research on the supply and demand of elderly care service resources in China. *Public Health Nurs.* **2024**, *41*, 1082–1088. [CrossRef] [PubMed]
26. Hu, H.; Shao, H.; Li, Y.; Guan, M.; Tong, J. GIS-Based Analysis of Elderly Care Facility Distribution and Supply-Demand Coordination in the Yangtze River Delta. *Land* **2025**, *14*, 723. [CrossRef]
27. Zhu, H. Spatial Matching and Policy-Planning Evaluation of Urban Elderly Care Facilities Based on Multi-Agent Simulation: Evidence from Shanghai, China. *Sustainability* **2022**, *14*, 16183. [CrossRef]
28. Wu, L.; Qian, L.; Li, Y.; Huang, Z.; Guan, W. Spatial coupling relationship between older adults and elderly care resources in the Yangtze River Delta. *PLoS ONE* **2023**, *18*, e293985. [CrossRef] [PubMed]
29. Li, H.; Li, R.; Cai, J.; Wang, S. The Spatial Equilibrium Model of Elderly Care Facilities with High Spatiotemporal Sensitivity and Its Economic Associations Study. *ISPRS Int. J. Geo-Inf.* **2024**, *13*, 268. [CrossRef]
30. Huang, X.; Gong, P.; White, M. Study on Spatial Distribution Equilibrium of Elderly Care Facilities in Downtown Shanghai. *Int. J. Environ. Res. Public Health* **2022**, *19*, 7929. [CrossRef] [PubMed]
31. Liu, L.; Lyu, H.; Dai, J.; Tu, Y.; Gao, T. Data-Driven Spatial Optimization of Elderly Care Facilities: A Study on Nonlinear Threshold Effects Based on XGBoost and SHAP—A Case Study of Xi'an, China. *ISPRS Int. J. Geo-Inf.* **2025**, *14*, 371. [CrossRef]
32. Zamfirescu-Mareș, D.; Corman, S. Depopulation, Ageing, and Social Sustainability: Institutionalized Elderly and the Geography of Care Between Rural and Urban Romania. *Sustainability* **2025**, *17*, 10419. [CrossRef]
33. Chen, H. Linking institutional function with form: Distributional dynamics, disequilibrium, and rural land shareholding in China. *Land Use Policy* **2022**, *120*, 106283. [CrossRef]
34. Theiss, M.; Szelewa, D. Institutional Sources of Citizens' Trust in the Welfare State: A Literature Review. *Soc. Policy Soc.* **2025**, *24*, 637–655. [CrossRef]
35. Li, B.; Long, J.; Li, Y. Geospatial analysis of healthcare and older adult care institutions in Wuhan: A multimethod approach to assessing spatial equity. *Front. Public Health* **2025**, *13*, 1580630. [CrossRef] [PubMed]
36. Zhang, Y.; Zhu, J.; Li, F.; Wang, Y. Site Selection of Elderly Care Facilities Based on Multi-Source Spatial Big Data and Integrated Learning. *ISPRS Int. J. Geo-Inf.* **2024**, *13*, 451. [CrossRef]
37. Li, M.; Peng, P.; Zhu, H.; Ao, Y.; Zhou, Z.; Long, Y.; Martek, I. Assessing the gap: Resource efficiency of institutionalised elderly care in urban and rural China. *Public Health* **2025**, *238*, 45–52. [CrossRef] [PubMed]
38. Wang, C.; Geng, X. Assessing the spatial equity of the aged care institutions based on the improved potential model: A case study in Shanghai, China. *Front. Public Health* **2024**, *12*, 1428424. [CrossRef] [PubMed]
39. Li, X.; Qin, W.; Jiang, H.; Qi, F.; Han, Z. Spatial equity and factors that influence the distribution of elderly care institutions in China. *Int. J. Health Geogr.* **2025**, *24*, 2. [CrossRef] [PubMed]
40. Li, M.; Peng, P.; Ao, Y.; Zhou, Z.; Zuo, J.; Martek, I. Equity in public decision-making: A dynamic comparative study of urban-rural elderly care institution resource allocation in China. *Humanit. Soc. Sci. Commun.* **2024**, *11*, 1526. [CrossRef]
41. Wang, M.; Qi, X.; Li, Z.; Li, J.; Dong, S. Evaluation of the suitability of elderly care in prefecture-level cities in China based on GIS. *Heliyon* **2023**, *9*, e16539. [CrossRef] [PubMed]
42. China Daily. Word of the Day|Common Prosperity for Everyone. 2020. Available online: https://language.chinadaily.com.cn/a/202011/04/WS5fa1fd10a31024ad0ba82ea5.html (accessed on 10 October 2026).
43. Xinhua. With the Aging of the Population, China is Accelerating the Reform of Elderly Care [In Chinese]. State Council of the People's Republic of China. 2025. Available online: https://english.www.gov.cn/news/202501/10/content_WS67805ca4c6d0868f4e8eea64.html (accessed on 10 October 2026).
44. Cheng, T.; Liu, C.; Yang, H.; Wang, N.; Liu, Y. From service capacity to spatial equity: Exploring a multi-stage decision-making approach for optimizing elderly-care facility distribution in the city centre of Tianjin, China. *Sustain. Cities Soc.* **2022**, *85*, 104076. [CrossRef]
45. Hu, Z.; Peng, X.; Wu, Y. The Chinese Strategy for Actively Responding to Population Ageing. *Soc. Sci. China* **2022**, *43*, 57–76. [CrossRef]
46. Cheng, K.; Liu, S.; Teng, M. Towards the Equalization of Basic Public Services in Chinese Cities: Investigating the Role of Urban Polycentric Structure. *Appl. Spat. Anal. Policy* **2025**, *18*, 143. [CrossRef]
47. Xu, J.; Liao, W.; Lim, N.H.H.; Fong, C.S.; Heng, C.K. A geostatistical diagnosis of eldercare facilities within the urban agglomeration: Exploring spatial (mis)match and service pressure in regional supply–demand dynamics. *J. Asian Archit. Build. Eng.* **2026**, 1–17. [CrossRef]
48. Rodríguez-Pose, A. The revenge of the places that don't matter (and what to do about it). *Camb. J. Reg. Econ. Soc.* **2018**, *11*, 189–209. [CrossRef]

49. Zhou, Y.; Zheng, W.; Wang, X. Polarisation or Equilibrium? The Impact of 'Core-Periphery' Interactions on Economic Efficiency in the Wuhan Metropolitan Area. *Tijdschr. Voor Econ. En. Soc. Geogr.* **2026**, *117*, 233–249. [CrossRef]
50. Liao, W.; Wu, D.; Guo, Z.; Zhao, C.; Xu, J.; Xu, Y. Variation analysis in historical demographic distribution within urban agglomeration: Experimental evidence from the Wuhan "1+8" City Circle. *Sustain. Soc. Dev.* **2024**, *2*, 2778. [CrossRef]
51. Zhou, Y.; Zheng, W.; Wang, X. Economic efficiency of the Wuhan metropolitan area under the interaction of urban hierarchy and population flow. *Prog. Geogr.* **2025**, *44*, 64–76. [CrossRef]
52. Liao, W.; Wang, H.; Xu, J. The Spatial Structure Characteristic and Road Traffic Accessibility Evaluation of A-Level Tourist Attractions within Wuhan Urban Agglomeration in China. *3C Tecnol.* **2024**, *12*, 388–409. [CrossRef]
53. Feng, Z.; Robinson, G.M.; Tan, Y. Rural Revitalization in China: Reversing Rural Decline and Eliminating Poverty. *Geogr. Compass* **2025**, *19*, e70039. [CrossRef]
54. Zhao, J.; Abdul Aziz, F.; Cheng, Z.; Ujang, N.; Zhang, H.; Xu, J.; Xiao, Y.; Shi, L. Post-Occupancy Evaluation of the Improved Old Residential Neighborhood Satisfaction Using Principal Component Analysis: The Case of Wuxi, China. *ISPRS Int. J. Geo-Inf.* **2024**, *13*, 318. [CrossRef]
55. Mitchell, A.; Griffin, L.S. The Esri Guide to GIS Analysis. In *Spatial Measurements and Statistics, Second Edition*; Esri Press: Redlands, CA, USA, 2021; Volume 2. Available online: https://www.esri.com/en-us/esri-press/browse/the-esri-guide-to-gis-analysis-volume-2-spatial-measurements-and-statistics-second-edition.html (accessed on 10 October 2026).
56. Xiao, Z.; Polat, M.; An, C. Spatial Distribution and Influencing Factors of Xinjiang Farmhouse Resorts: An Analysis Based on POI Data. *J. Southwest Univ.* **2022**, *44*, 144–154. [CrossRef]
57. Sun, J.; Tian, Y.; Cui, J.; Luo, J.; Zeng, J.; Han, Y. Identification of Tourism Spatial Structure and Measurement of Tourism Spatial Accessibility in Hubei Province. *Econ. Geogr.* **2017**, *37*, 208–217. [CrossRef]
58. De Mello-Sampayo, F. Spatial and Temporal Analysis of COVID-19 in the Elderly Living in Residential Care Homes in Portugal. *Int. J. Environ. Res. Public Health* **2022**, *19*, 5921. [CrossRef] [PubMed]
59. Xu, J.; Wang, H.; Liao, W.; Fong, C.S. From Closure to Gradual Release: Evidence from the Spatial Evolution and Causal Mechanism of EGS Industry in the Main Town Area of Wuhan, China. *3C Empresa* **2023**, *12*, 15–37. [CrossRef]
60. Song, H.; Meng, Q.; Wang, C. Spatial Distribution Characteristics and the Evolution of Buddhist Monasteries in Xi'an City Area. *Religions* **2023**, *14*, 1084. [CrossRef]
61. Xu, J.; Peng, W.; Lim, N.H.H.; Liao, W.; Fong, C.S. Intangible Cultural Heritage in Territorial Space: Historical Trend Characteristics and Development Strategic Routes. In *Geographic Information Systems for Urban Identity, Morphology and Transformation: Bridging the Gap Between Urban Space and Heritage Changes*; Ripp, M., Vileikis, O., Majumdar, S., Eds.; Springer Nature: Cham, Switzerland, 2026; pp. 117–139. [CrossRef]
62. Silverman, B.W. *Density Estimation for Statistics and Data Analysis*, 1st ed.; Routledge: Abingdon, UK, 2018. [CrossRef]
63. ESRI. How Kernel Density Works. 2026. Available online: https://desktop.arcgis.com/en/arcmap/latest/tools/spatial-analyst-toolbox/how-kernel-density-works.htm (accessed on 10 October 2026).
64. Wikipedia. Kernel Density Estimation. 2026. Available online: https://en.wikipedia.org/wiki/Kernel_density_estimation (accessed on 30 October 2026).
65. Levin, N.; Levine, N. CrimeStat III—A Spatial Statistics Program for the Analysis of Crime Incident Locations. US National Institute of Justice; 2004. Available online: https://www.ojp.gov/ncjrs/virtual-library/abstracts/crimestat-iii-spatial-statistics-program-analysis-crime-incident (accessed on 30 October 2026).
66. Chainey, S.; Ratcliffe, J. *GIS and Crime Mapping*; Wiley: Hoboken, NJ, USA, 2005. [CrossRef]
67. Levine, N. CrimeStat: A Spatial Statistical Program for the Analysis of Crime Incidents. In *Encyclopedia of GIS*; Shekhar, S., Xiong, H., Zhou, X., Eds.; Springer International Publishing: Cham, Switzerland, 2017; pp. 381–388. [CrossRef]
68. Burman, P.; Nolan, D. Location-adaptive density estimation and nearest-neighbor distance. *J. Multivar. Anal.* **1992**, *40*, 132–157. [CrossRef]
69. Williamson, D.; McLafferty, S.; Goldsmith, V.; Mollenkopf, J.; McGuire, P. A better method to smooth crime incident data. In *ESRI ArcUser Online*; ESRI: Redlands, CA, USA, 2026. Available online: https://www.esri.com/news/arcuser/0199/crimedata.html (accessed on 30 October 2026).
70. Ye, X.; Fan, Y.; Miao, J.; He, Z. The Competitiveness of Regional Urban System in Hubei Province of China. *Land* **2022**, *11*, 879. [CrossRef]
71. Jiang, L.; Chen, J.; Zhang, C.; Tian, Y.; Wu, G.; Luo, J. Study on spatial evolution and mechanism of county economic differences in Hubei province from 2005 to 2020. *Front. Earth Sci.* **2022**, *10*, 918123. [CrossRef]
72. Brenner, N. *New Urban Spaces: Urban Theory and the Scale Question*; Oxford University Press: Oxford, UK, 2019. [CrossRef]
73. Brenner, N. *New State Spaces: Urban Governance and the Rescaling of Statehood*; Oxford University Press: Oxford, UK, 2004. [CrossRef]
74. Lin, S.; Liu, X.; Wang, T.; Li, Z. Revisiting entrepreneurial governance in China's urban redevelopment: A case from Wuhan. *Urban Geogr.* **2023**, *44*, 1520–1540. [CrossRef]

75. Ding, W.; Xu, G.; Xu, J.; Matsubara, S.; Ma, R.; Ma, M.; Li, H. Multi-Dimensional Accessibility Framework for Nursing Home Planning: Insights from Kunming, China. *Sustainability* **2025**, *17*, 7606. [CrossRef]
76. Li, J.; Cheng, X.; Jin, S.; Zheng, Y. Sustainable Provision of Community-Based Eldercare Facilities in High-Density Cities: A Four-Dimensional Spatial Evaluation Framework Integrating Governance, Market, and Users. *Sustainability* **2026**, *18*, 9386. [CrossRef]
77. Lu, G.; Wang, L.; Jiao, Y.; Du, P. Evaluation and optimization of spatial equity in elderly care facilities: A case study of Dalian, China. *Humanit. Soc. Sci. Commun.* **2026**, *13*, 168. [CrossRef]
78. Kostilainen, H.; Karjalainen, J. Institutional and territorial drivers of rural social enterprise ecosystems: Evidence from Finland. *Soc. Entrep. Rev.* **2025**, *2*, 137–151. [CrossRef]
79. Mazzei, M. Understanding difference: The importance of 'place' in the shaping of local social economies. *Volunt. Int. J. Volunt. Nonprofit Organ.* **2017**, *28*, 2763–2784. [CrossRef]
80. Plata, G.; Scott, S.; Aparicio, S. Fostering an environment for social entrepreneurship: A comparative analysis across economic development levels. *Rev. Manag. Sci.* **2026**, *20*, 135–168. [CrossRef]
81. Xu, F.; Lawson, J. Eldercare and re-purposing the built environment of urban China: Capital switching and bundled commodities in recent trends. *Hum. Geogr.* **2026**, *19*, 217–231. [CrossRef] [PubMed]
82. Huang, G.; Ma, J.; Wang, J. Spatial justice in the Silver Economy: Determinants and spillover effects of elderly care resources in China. *Humanit. Soc. Sci. Commun.* **2026**, *13*, 1947. [CrossRef]
83. Tai, H.Y. The Welfare Stratification of Aging Population in Urban China. Master's Thesis, National Tsing Hua University, Hsinchu, China, 2015.
84. Yu, Y. Towards a critical geography of aging: Political economy, biopolitics, and care. *Prog. Hum. Geogr.* **2025**, *49*, 164–181. [CrossRef]
85. Razavi, S. The Political and Social Economy of Care in a Development Context: Conceptual Issues, Research Questions and Policy Options. 2007. Available online: https://repositorio.unal.edu.co/handle/unal/47163 (accessed on 30 October 2026).
86. Song, J.; Yuan, H.; Nie, R. Combination of Effective Government and Efficient Market in Regional Equalization of Basic Public Services: Evidence Based on Government Investment and Private Investment. *Chin. J. Manag. Sci.* **2025**, *33*, 95–107. [CrossRef]
87. Bi, X.; Li, M. Equity versus efficiency: A spatial analysis of residential aged care resources in Beijing. *Chin. J. Sociol.* **2023**, *9*, 127–158. [CrossRef]
88. Guo, L.; Wei, H.; Tao, Q.; Chen, K. Coupling coordination evaluation and influencing factors analysis of older adult care service resource supply and demand in China. *Front. Public Health* **2025**, *13*, 1662064. [CrossRef] [PubMed]
89. Ministry of Civil Affairs of the People's Republic of China. Notice of the Ministry of Civil Affairs on Issuing the Guidelines for the Construction and Management of Urban-Rural Three-Tier Elderly Care Service Networks. 2026. Available online: https://www.mca.gov.cn/n152/n165/c1662004999980011819/content.html (accessed on 30 October 2026).
90. China Daily. Plans for Three-Tier Eldercare Network: System to Extend from Urban Centers to Remote Rural Communities by 2029. 2026. Available online: https://en.humanrights.cn/2026/07/13/d3bee254a2b546cc9bec6d6302013b33.html (accessed on 30 October 2026).
91. Jiang, C. Optimization of spatial layout of community elderly care facilities based on supply and demand matching. *Bull. Surv. Mapp.* **2025**, *5*, 119–124. [CrossRef]
92. Li, X. A Place of Integration or Segregation? Analysing the Multi-Scale Social and Spatial Configuration of Elderly Care Facilities in Communities. Doctoral Dissertation, University College, London, UK, 2026.

Disclaimer/Publisher's Note: The statements, opinions and data contained in all publications are solely those of the individual author(s) and contributor(s) and not of MDPI and/or the editor(s). MDPI and/or the editor(s) disclaim responsibility for any injury to people or property resulting from any ideas, methods, instructions or products referred to in the content.